Immobility-associated thromboprotection is conserved across mammalian species from bear to human

Article

Accepted Version

Title: Immobility-associated thromboprotection is conserved across mammalian species from bear to human

Authors

Manuela Thienel*[1,2], Johannes B. Müller-Reif*[3,4], Zhe Zhang*[1], Vincent Ehreiser[1,2], Judith Huth[1,2], Khrystyna Shchurovska[1,2], Badr Kilani[1,2], Lisa Schweizer[3], Philipp E. Geyer[3,4], Maximilian Zwiebel[3], Julia Novotny[1], Enzo Lüsebrink[1], Gemma Little[5], Martin Orban[1], Leo Nicolai[1,2], Shaza El Nemr[1,2], Anna Titova[1,2], Michael Spannagl[6], Jonas Kindberg[7,8], Alina L. Evans[9], Orpheus Mach[10], Matthias Vogel[10], Steffen Tiedt[11], Steffen Ormanns[12], Barbara Kessler[13], Anne Dueck[2,14], Andrea Friebe[7,8], Peter Godsk Jørgensen[15], Monir Majzoub-Altweck[16], Andreas Blutke[16], Amin Polzin[17], Konstantin Stark[1,2], Stefan Kääb[1,2], Doris Maier[10], Jonathan M Gibbins[5], Ulrich Limper[18,19], Ole Frobert[20,21,22,23#], Matthias Mann[3,#], Steffen Massberg[1,2,#], Tobias Petzold[1,2#]

[1] Department of Cardiology, University Hospital, LMU Munich, 81377 Munich, Germany

[2] DZHK (German Centre for Cardiovascular Research), partner site Munich Heart Alliance, 80802 Munich, Germany

[3] Department of Proteomics and Signal Transduction, Max Planck Institute of Biochemistry, 82152 Martinsried, Germany

[4] Omicera Diagnostics, 82152 Martinsried, Germany

[5] Institute for Cardiovascular and Metabolic Research, School of Biological Sciences, Health and Life Sciences Building, University of Reading, RG6 6UR, United Kingdom

[6] Anesthesiology and Transfusion Medicine, Cell Therapeutics and Hemostaseology, Ludwig-Maximilians-University Munich, 80336 Munich, Germany

[7] Norwegian Institute for Nature Research, 7034 Trondheim, Norway

[8] Scandinavian Brown Bear Research Project

[9] Department of Forestry and Wildlife Management, Faculty of Applied Ecology and Agricultural Sciences, Inland Norway University of Applied Sciences, 2480 Koppang, Norway.

[10] Zentrum für Rückenmarkverletzte mit Neuro-Urologie, BG Unfallklinik Murnau, 82418 Murnau am Staffelsee, Germany

[11] Neurologische Klinik und Poliklinik, Klinikum der Universität München, Ludwig-Maximilians-University Munich, 81377 Munich, Germany

[12] Pathologisches Institut, Klinikum der Universität München, Ludwig-Maximilians- University Munich, 81377 Munich, Germany

[13] Gene Center, Ludwig-Maximilians- University Munich, 81377 Munich, Germany

[14] Institute of Pharmacology and Toxicology, Technical University of Munich, 80802 Munich, Germany

[15] Herlev and Gentofte University Hospital, Borgmester Ib Juuls Vej 1, DK-2730, Herlev, Copenhagen, Denmark.

[16] Institute of Veterinary Pathology, Center for Clinical Veterinary Medicine, LMU Munich, 80539 Munich, Germany

[17] Division of Cardiology, Pulmonology, and Vascular Medicine, Heinrich Heine University Medical Center Dusseldorf, 40225 Dusseldorf, Germany

[18] Institute of Aerospace Medicine, German Aerospace Center (DLR), 51147 Cologne, Germany

[19] Department of Anesthesiology and Intensive Care Medicine, Merheim Medical Center, Hospitals of Cologne, University of Witten/Herdecke, 51109 Cologne, Germany

[20]Faculty of Health, Department of Cardiology, Örebro University, 701 85 Örebro, Sweden;

[21]Department of Clinical Medicine, Faculty of Health, Aarhus University, 8000 Aarhus, Denmark.

[22]Department of Clinical Pharmacology, Aarhus University Hospital, 8000 Aarhus, Denmark.

[23]Steno Diabetes Center Aarhus, Aarhus University Hospital, 8000 Aarhus, Denmark

* contributed equally as first author

Corresponding authors

E-mail: tobias.petzold@med.uni-muenchen.de, Tel: +49 177 4202593

steffen.massberg@med.uni-muenchen.de

mmann@biochem.mpg.de

ole.frobert@regionorebrolan.se

Abstract

Venous thromboembolism (VTE) comprising deep venous thrombosis and pulmonary embolism is a major cause of morbidity and mortality. Short-term immobility-related conditions are a major risk factor for the development of VTE. Paradoxically, long-term immobilized free-ranging hibernating brown bears and paralyzed spinal cord injury (SCI) patients are protected from VTE. Here we aimed to identify mechanisms of immobility-associated VTE protection in a cross-species approach. Mass spectrometry-based proteomics revealed an antithrombotic signature in platelets of hibernating brown bears with heat shock protein 47 (HSP47) as most substantially reduced protein. HSP47 downregulation or ablation attenuated immune cell activation and NET formation, contributing to thromboprotection in bears, SCI patients and mice. This cross-species conserved platelet signature may give rise to antithrombotic therapeutics and prognostic markers beyond immobility-associated VTE.

One sentence summary: Long-term immobility induces an antithrombotic platelet signature reducing thromboinflammation and thrombosis risk.

Main text

Immobilization is a major risk factor for the development of venous thromboembolism (VTE) causing tremendous socioeconomic costs (*1*). Immobility-associated VTE is initiated by flow restriction in veins causing endothelial cell hypoxia (*2*). Recruitment of platelets to the activated endothelium leads to local activation of the plasmatic coagulation system and innate immune cells (for example neutrophils and monocytes), orchestrating deleterious thromboinflammation, the central mechanism of VTE (*3, 4*). Despite long-term immobilization chronically paralyzed patients with spinal cord injury exhibit a VTE risk similar to that of the general population (*5-7*). Hibernating brown bears *(Ursus arctos)* are another example of an organism with a period of long-term immobilization during winter. While hibernating bears enter a physically immobile state that is accompanied by a drastically reduced cardiac output, there is no obvious evidence for VTE (*8-11*). In our present study, we identified a platelet-derived antithrombotic molecular signature that is conserved across different species and protects from immobility-induced VTE.

Results

VTE in non-hibernating brown bears

Immobilization is a major risk factor linked to increased rates of VTE even in the absence of additional health care related factors, such as obesity, acute trauma or medical interventions (*1, 12*). Yet, hibernation of some animal species leads to immobilization for several weeks or months. During their annual 4- to 7-month-long hibernation episodes, brown bears show remarkable plasticity by establishing an energy saving metabolism to adapt to hostile environmental changes during winter. Though, this has not been linked to increased VTE-associated complications. A case in point are the Swedish brown bears with a mortality rate during hibernation of only 0.4 % compared to 58.4 % during activity (Figure S1A). In these bears we found no echocardiographic evidence of pulmonary embolism during hibernation (right ventricle diameter, Figure S1B) and D-dimer levels were reduced compared to active bears (Figure 1A). This indicates that immobilization during hibernation is not linked to an obvious excess in VTE rates. Nevertheless, non-hibernating brown bears may develop VTE (Table S1). Analysis of autopsy samples revealed characteristic histological pulmonary thrombus structure in some bears, including intravascular neutrophil extracellular traps (NETs), prothrombogenic externalized nuclear DNA-histone strands that foster intravascular thrombosis (28, 29) (Figure 1B-C). By spatial proteomics of thrombus samples, we identified key components of the coagulation system (for example factor X, factor V), platelets (for example glycoprotein (GP)V, GPIbα) and neutrophils (for example neutrophil elastase) in both brown bears and patients with VTE (Figure 1D-E, Table S2). Thus, brown bears possess a thromboinflammatory machinery similar to humans enabling them to develop VTE, but appear to be protected from immobility-associated VTE during hibernation.

Antithrombotic platelet signatures during hibernation

To identify factors potentially contributing to a naturally occurring antithrombotic mechanism during hibernation, we serially captured thirteen subadult brown bears for blood sampling during hibernation and the following activity period in spring in middle Sweden (Figure 2A). First, we performed hematological characterization of the Scandinavian brown bear cohort. Hemoglobin and hematocrit values were elevated during winter reflecting intravascular dehydration (*13*) (Figure S2A). Whole blood thromboelastographic analysis showed that clot formation upon activation of the intrinsic but not of the extrinsic coagulation pathway is delayed during inactivity (Figure 2B), even when we adjusted for seasonal differences in body temperatures (winter 33°C, summer 37°C). Thrombus mass (clot firmness) was mildly reduced during hibernation (Figure 2B).

Population-based studies have associated plasma coagulation factor activities with VTE risk in humans (*14, 15*). When characterizing alterations within the intrinsic coagulation pathway of the bears in more detail, we found a prolonged plasma clotting time (aPTT), yet with values that were still within the human reference range (*16*) (Figure S2B), and single coagulation factor (factor VIII, factor IX, factor XI, factor XII) function was also only mildly reduced during winter (Figure S2C). Mass spectrometry (MS)-based plasma proteome profiling (*17*) showed no major differences in coagulation-related plasma proteins between active state and hibernation. Instead, plasma proteome differences were dominated by enzymes that reflected a seasonal switch in metabolism, dominating intra-individual differences (Figure S2D-F). Seasonal alterations in coagulation factors therefore are not the main feature responsible for VTE protection during hibernation. Instead, thromboelastography revealed that the seasonal differences in clot formation depend on platelets and disappear after platelet inhibition (FIBTEM, Figure 2B). Of note, plasma levels of the physiological endothelial cell derived platelet inhibitor prostacyclin were reduced during winter (Figure S2G). This prompted us to focus on the characterization of the platelet population as the central blood component regulating physiological hemostasis and pathological thrombosis.

Platelet and neutrophil counts were reduced (by 37.9% and 20.9%, respectively) in winter compared to summer (Figure S2A). The changes in platelets and neutrophils were mild compared to other well-studied hibernating animals such as hamsters and other rodents in which a drastic decrease of body temperature below 10°C leads to profound sequestering of platelets in the liver, neutrophil margination to the vessel wall, and lymphocyte storage in secondary lymphoid organs (*18-20*). To analyze seasonal platelet function on a single cell type level adjusted for the differences in platelet counts, we freshly isolated washed platelets. In winter compared to summer, platelet aggregation was delayed and reduced upon stimulation with fibrillar collagen and low but not high doses thrombin (Figure 2C), while ADP, Thromboxane A analog U46619, and Thrombin receptor activating peptide (TRAP) induced platelet-shape change but failed to trigger platelet aggregation (Figure S2H). Platelet aggregation is accompanied by the release of the platelet granule compartment, fostering aggregation by providing auto- and paracrine acting platelet agonists and fibrinogen as crosslinking substrate (*21, 22*). Using MS-based proteomics we found attenuated platelet protein release in response to collagen during winter compared to summer (Figure 2D, Figure S2I). Spreading of individual collagen-activated platelets on soluble collagen and fibronectin, the substrates of α2β1 and α5β1 integrin adhesion receptors, was reduced in winter compared to summer. In contrast, we did not detect significant seasonal differences in platelet spreading in response to thrombin or on fibrinogen, the substrate of the most abundantly expressed platelet integrin $\alpha IIb\beta_3$ (Figure 2E, Figure S3A-C). These data show that collagen- and thrombin-induced platelet signaling during hibernation is attenuated, affecting distinct platelet responses.

To elucidate the molecular basis of reduced platelet reactivity towards collagen and thrombin during inactivity, we again chose MS-based proteomics, as it only requires that the species has a sequenced genome, but no active transcription and translation or available antibodies are necessary as in affinity-based protein identification (*23, 24*). This technology has successfully been applied to biomarker discovery on body fluids and derived cell types, including platelets (*25, 26*). Despite poor annotation of the bear genome, we identified and quantified more than 2678 proteins. Platelet proteomes are markedly different between

hibernating and active brown bears, with the abundance of 151 proteins (5.6%) significantly (FDR < 5 %) changing with an absolute average of 2.1-fold. Of these, 80 were expressed at lower levels and 71 at higher levels during inactivity (Figure 2F). The Gene Ontology (GO) terms associated with catabolism such as 'proteolysis', 'peptidase activity' and 'proteasome complex' were enriched in the more highly expressed platelet proteins during inactivity, whereas no specific term enrichment was seen in the less expressed proteins (FDR < 0.02). Focusing on proteins involved in platelet activation, we found decreased amounts of ROCK1 (Rho-associated coiled-coil-containing protein kinase 1) during inactivity. ROCK1 is regulated by the small Rho-GTPase RhoA, and two of its activating guanidine exchange factors (GEFs) FYVE and DOCK6 were also downregulated, whereas ARHGAP1, a deactivator, was upregulated. These findings already indicated a seasonal functional conversion of the platelet proteome towards lower activity. However, the platelet protein with the largest difference between hibernating and active bears was the gene product of SERPINH1, also known as heat shock protein 47 (HSP47). On average, HSP47 was 55-fold downregulated in the platelets of hibernating bears, ten times more than the next most down regulated protein (RRBP1, five-fold-change) (Figure 2F-I).

Platelet HSP47 regulates thromboinflammation

HSP47 belongs to the serine proteinase inhibitor (serpin) superfamily but possesses no serine protease inhibitory activity. In a fibroblast context it acts as an endoplasmic reticulum resident chaperone, specifically facilitating collagen folding and secretion into the extracellular space. In different fibrotic diseases and skeletal malformation pathologies, HSP47 acts as a key disease driver (*27*). Recently, it has been detected on the platelet membrane, promoting collagen signaling together with GPVI and integrin α2β1, the two major collagen receptors in experimental arterial thrombosis and stroke (*28-31*).

Given its strong regulation and cross-species conservation, we decided to functionally investigate the potential protective effect of HSP47 downregulation in the context of VTE.

To define the functional role of platelet HSP47 in VTE in vivo, we generated *PF4-Cre(+)/HSP47*$^{-/-}$ or *PF4-Cre(-)/HSP47*$^{fl/fl}$ bone marrow chimeric mice and subjected them to venous flow restriction (Figure 3A, figure S4A, B). HSP47 is abundantly expressed by platelets, but not by leukocytes. *PF4-Cre* mediated recombination in chimeric mice therefore leads to specific deletion of HSP47 in the platelet compartment (Figure 3B, Figure S4C). Thrombus frequency and sizes in *PF4-Cre(+)/HSP47*$^{-/-}$ chimeric mice were drastically reduced compared to controls (Figure 3C). At the same time, NETs were reduced in *PF4-Cre(+)/HSP47*$^{-/-}$ compared with control mice (Figure 3D). As patients with VTE have increased plasma levels of NET markers, we also quantified circulating citH3/DNA complexes (Figure 3E) as well as circulating DNA (Figure S4D) in bears (*32-34*). Along with Hsp47 downregulation and D-dimer levels (Figure 1A), both markers were reduced during hibernation. Consistent with these findings we observed reduced prothrombotic NET formation in an in vitro co-culture model of neutrophils and platelets isolated from hibernating compared to active brown bears, while NET formation of PMA-stimulated neutrophils was unaffected (Figure 3F). When we pretreated human platelets with two HSP47-specific small molecule inhibitors (SMI; Col003, SMI II; RH00007SC)(*28, 35*), platelet-neutrophil aggregates were reduced upon stimulation with thrombin (Figure 3G, Figure S4E) and prothrombotic NET formation was attenuated (Figure 3H, Figure S4F).

Activated platelets fuel NET formation by release of granule content and direct physical interactions with neutrophils (*36, 37*). To dissect the functional role of HSP47 in both processes, we first quantified platelet activation and granule release by multi-color flow cytometry. SMI I treatment reduced the fraction of activated platelets that express high levels of granule secretion markers (CD62P^{high}, CD63^{high}) as well as active integrin αIIbβ3 (PAC-1^{high}) and attenuated collagen platelet aggregation (t-SNE cluster population 5; Figure 4A, figures S5A-C). In phospho-proteome analysis of aggregation assays, phosphorylation patterns were sensitive to HSP47 inhibition with SMI I (Figure 4B, figure S5D-G) as well as SMI II (Figure S5H). Pharmacological inhibition of HSP47 with SMIs almost completely abolished binding of thrombin

to the platelet surface (Figure 4C). We also found reduced thrombin binding to HSP47-deficient mouse platelets (Figure 4D), suggesting that HSP47 regulates thrombin recruitment to platelet surfaces.

Next, we investigated whether the interaction of HSP47 with neutrophils impacts their function. Flow cytometric analysis of neutrophils treated with purified HSP47 revealed increased intracellular reactive oxygen species production and increased leukocyte integrin CD11b expression, only somewhat less efficient than N-Formylmethionine-leucyl-phenylalanine (fMLP), an established highly potent neutrophil activator (Figure 4E-F). Direct or co-stimulation with HSP47 augmented NET formation even in the absence of platelets (Figure 4G). To further elucidate the molecular mechanism by which HSP47 activates neutrophils, we analyzed toll-like receptor (TLR) signaling, which is known to be induced by other heat shock proteins. Indeed, inhibition of TLR2 but not TLR4 reduced CD11b expression in response to HSP47 peptide (Figure 4H-I). In line with this, we found reduced CD11b expression after inhibition of MyD88 by Pepinh-MYD peptide, a canonical adaptor downstream of TLR-2 and -4 signaling pathway, after stimulation with recombinant HSP47 (Figure 4J). In summary, we identified a mechanism by which HSP47 facilitates thrombin binding to platelet surfaces as well as neutrophil activation via the TLR2-MyD88 signaling axis.

HSP47 downregulation in immobile patients

We addressed the relevance of thromboprotective HSP47 down-regulation in scenarios beyond hibernation. Chronically paralyzed patients with spinal cord injury (SCI) exhibit a VTE risk similar to the general population for unknown reason despite long term immobilization (*5-7*). We therefore recruited chronically immobilized patients who were either bedridden or wheelchair-bound due to SCI and matched healthy controls (Figure 5A, Table S3). HSP47 levels before SCI were unknown, but platelet HSP47 expression was reduced in SCI compared to matched healthy controls, parallel to the hibernating bear population. The expression of other key platelet receptors (GPVI and GPIbα) remained unchanged, indicating a specific response (Figure 5B, figure S6A). Immunoblotting and confocal fluorescence microscopy confirmed reduced protein expression while HSP47 cellular distribution did not differ (Figure 5C-D). Coagulation and

whole blood thrombus formation was unchanged between patients and controls (Figure S6B, C). Circulating DNA and citrullinated histone 3 levels, biomarkers of NET formation, were also similar, indicating absence of a pro-thrombotic state in chronically immobilized patients (Figure S6D). Consistent with our findings regarding human platelets treated with HSP47 SMI, thrombin binding to platelets was reduced in SCI patients (Figure 5E). Quantifying agonist-induced platelet activation indicated normal aggregation responses (Figure S6E) while platelet granule release and integrin activation (i.e. CD62P and PAC-1) were attenuated in chronic immobilization (Figure 5F). The reduced HSP47 levels on SCI platelets were associated with attenuated neutrophil platelet interactions and NETosis compared to healthy controls (Figure 5G-I). A merged analysis of both groups revealed a direct correlation between HSP47 expression and platelet neutrophil aggregates or NETs (Figure 5J), indicating that HSP47 expression correlates with thrombogenicity in immobilized patients. When we analyzed *HSP47* mRNA in platelets, we found reduced *HSP47* transcripts in SCI patients compared to healthy controls, indicating that HSP47 regulation occurs at the megakaryocyte (MK) level (Figure 5K). In patients acutely immobilized with intracranial bleeding (Table S4), the kinetics of platelet HSP47 downregulation but not GPVI or GPIbα level followed platelet turnover, consistent with a regulation of HSP47 expression at the MK level (Figure S6F).

Finally, to study the effect of immobilization in a physiological setting, we analyzed a longitudinal cohort of healthy individuals undergoing voluntary bed rest immobilization (see methods, Figure 5L). After 27 days of bed rest, platelet HSP47 was drastically reduced while GPVI or GPIbα surface expression did not change (Figure 5M, figure S6G-H). In a metaproteome analysis, we performed a bioinformatic matching for homologous proteins between the human and bear proteome (Figure 5N, Table S5). This enabled a cross species comparison of immobility-induced proteome changes, where we focused on proteins involved in platelet activation. In addition to HSP47 we observed a downregulation of SYK, ASAP1, Erp44 upon immobility in bears and humans. All of these proteins are known to be involved in platelet activation (*38-40*). We conclude that immobility is a trigger for functional platelet proteome conversion in an antithrombotic manner. To explore immobility-induced HSP47 downregulation in platelets across a wider

range of species, we added pigs as another mammalian model. After giving birth to their piglets lactating pigs were limited in mobility for 21-28 days. Compared to free-ranging indoor pigs platelet HSP47 expression was reduced as detected using flow-cytometry (Figure 5O). However, mobile pigs were neither lactating nor gave birth within the last weeks which is a limiting factor, that might affect HSP47 expression.

Discussion

Combining functional analyses in free-ranging brown bears, mice, pigs, and humans, we uncovered a cross-species conserved physiological process upon immobilization. Via HSP47 downregulation, chronic immobilization conveys protection from VTE by reversing the pro-thromboinflammatory state that normally follows immobilization. We therefore suggest that HSP47 is a promising target to prevent VTE in patients exposed to immobilization, that might be evolutionarily conserved across mammals. Our findings provide mechanistic insight into the paradox that the VTE risk of long-term immobilized SCI patients resembles the risk of the general population. It will be interesting to further investigate the molecular basis of mechanosensation during hemostasis and thrombosis in various contexts, including microgravity in space, which can lead to venous thrombosis (*41, 42*). However, our data also establish a function of HSP47 driving thromboinflammation in the tightly controlled interplay of innate immune cells and platelets in general. Towards clinical application, our findings thus suggest a concept for treating thromboinflammatory cardiovascular diseases by making use of naturally occurring thromboprotective mechanisms.

Immobility is not the single cause of VTE, and we did not investigate the role of HSP47 in other thromboembolic environments such as cancer or coagulation disorders. Nevertheless, patients at risk of VTE beyond immobilization might benefit from treatments mimicking the here described thromboprotective mechanism.

References and notes

1. F. Khan, T. Tritschler, S. R. Kahn, M. A. Rodger, Venous thromboembolism. *Lancet* **398**, 64-77 (2021).
2. K. Stark, S. Massberg, Interplay between inflammation and thrombosis in cardiovascular pathology. *Nat Rev Cardiol* **18**, 666-682 (2021).
3. M. L. von Bruhl *et al.*, Monocytes, neutrophils, and platelets cooperate to initiate and propagate venous thrombosis in mice in vivo. *J Exp Med* **209**, 819-835 (2012).
4. B. Engelmann, S. Massberg, Thrombosis as an intravascular effector of innate immunity. *Nat Rev Immunol* **13**, 34-45 (2013).
5. L. N. Godat, L. Kobayashi, D. C. Chang, R. Coimbra, Can we ever stop worrying about venous thromboembolism after trauma? *J Trauma Acute Care Surg* **78**, 475-480; discussion 480-471 (2015).
6. M. Giorgi Pierfranceschi *et al.*, The short- and long-term risk of venous thromboembolism in patients with acute spinal cord injury: a prospective cohort study. *Thromb Haemost* **109**, 34-38 (2013).
7. R. A. Maxwell *et al.*, Routine prophylactic vena cava filtration is not indicated after acute spinal cord injury. *J Trauma* **52**, 902-906 (2002).
8. O. Frobert, A. M. Frobert, J. Kindberg, J. M. Arnemo, M. T. Overgaard, The brown bear as a translational model for sedentary lifestyle-related diseases. *J Intern Med* **287**, 263-270 (2020).
9. P. G. Jorgensen *et al.*, Low cardiac output as physiological phenomenon in hibernating, free-ranging Scandinavian brown bears (Ursus arctos) - an observational study. *Cardiovasc Ultrasound* **12**, 36 (2014).
10. A. U. Friedrich *et al.*, Comparative coagulation studies in hibernating and summer-active black bears (Ursus americanus). *Thromb Res* **158**, 16-18 (2017).
11. T. L. Iles, T. G. Laske, D. L. Garshelis, P. A. Iaizzo, Blood clotting behavior is innately modulated in Ursus americanus during early and late denning relative to summer months. *J Exp Biol* **220**, 455-459 (2017).
12. M. J. Engbers, J. W. Blom, M. Cushman, F. R. Rosendaal, A. van Hylckama Vlieg, The contribution of immobility risk factors to the incidence of venous thrombosis in an older population. *J Thromb Haemost* **12**, 290-296 (2014).
13. K. G. Welinder *et al.*, Biochemical Foundations of Health and Energy Conservation in Hibernating Free-ranging Subadult Brown Bear Ursus arctos. *J Biol Chem* **291**, 22509-22523 (2016).
14. J. C. Meijers, W. L. Tekelenburg, B. N. Bouma, R. M. Bertina, F. R. Rosendaal, High levels of coagulation factor XI as a risk factor for venous thrombosis. *N Engl J Med* **342**, 696-701 (2000).
15. M. Cushman, E. S. O'Meara, A. R. Folsom, S. R. Heckbert, Coagulation factors IX through XIII and the risk of future venous thrombosis: the Longitudinal Investigation of Thromboembolism Etiology. *Blood* **114**, 2878-2883 (2009).
16. S. M. Bates, J. I. Weitz, Coagulation assays. *Circulation* **112**, e53-60 (2005).
17. P. E. Geyer *et al.*, Plasma Proteome Profiling to Assess Human Health and Disease. *Cell Syst* **2**, 185-195 (2016).
18. B. Sahdo *et al.*, Body temperature during hibernation is highly correlated with a decrease in circulating innate immune cells in the brown bear (Ursus arctos): a common feature among hibernators? *Int J Med Sci* **10**, 508-514 (2013).
19. H. R. Bouma *et al.*, Low body temperature governs the decline of circulating lymphocytes during hibernation through sphingosine-1-phosphate. *Proc Natl Acad Sci U S A* **108**, 2052-2057 (2011).
20. H. R. Bouma *et al.*, Reduction of body temperature governs neutrophil retention in hibernating and nonhibernating animals by margination. *J Leukoc Biol* **94**, 431-437 (2013).

21. J. A. Coppinger *et al.*, Characterization of the proteins released from activated platelets leads to localization of novel platelet proteins in human atherosclerotic lesions. *Blood* **103**, 2096-2104 (2004).
22. S. R. Piersma *et al.*, Proteomics of the TRAP-induced platelet releasate. *J Proteomics* **72**, 91-109 (2009).
23. J. B. Muller *et al.*, The proteome landscape of the kingdoms of life. *Nature* **582**, 592-596 (2020).
24. M. Heck, B. A. Neely, Proteomics in Non-model Organisms: A New Analytical Frontier. *J Proteome Res* **19**, 3595-3606 (2020).
25. M. Zeiler, M. Moser, M. Mann, Copy number analysis of the murine platelet proteome spanning the complete abundance range. *Mol Cell Proteomics* **13**, 3435-3445 (2014).
26. P. E. Geyer, L. M. Holdt, D. Teupser, M. Mann, Revisiting biomarker discovery by plasma proteomics. *Mol Syst Biol* **13**, 942 (2017).
27. S. Ito, K. Nagata, Roles of the endoplasmic reticulum-resident, collagen-specific molecular chaperone Hsp47 in vertebrate cells and human disease. *J Biol Chem* **294**, 2133-2141 (2019).
28. P. Sasikumar *et al.*, The chaperone protein HSP47: a platelet collagen binding protein that contributes to thrombosis and hemostasis. *J Thromb Haemost* **16**, 946-959 (2018).
29. W. J. Kaiser, L. M. Holbrook, K. L. Tucker, R. G. Stanley, J. M. Gibbins, A functional proteomic method for the enrichment of peripheral membrane proteins reveals the collagen binding protein Hsp47 is exposed on the surface of activated human platelets. *J Proteome Res* **8**, 2903-2914 (2009).
30. T. Petzold *et al.*, beta1 integrin-mediated signals are required for platelet granule secretion and hemostasis in mouse. *Blood* **122**, 2723-2731 (2013).
31. S. Wu *et al.*, Hsp47 Inhibitor Col003 Attenuates Collagen-Induced Platelet Activation and Cerebral Ischemic-Reperfusion Injury in Rats. *Front Pharmacol* **12**, 792263 (2021).
32. M. Jimenez-Alcazar, N. Kim, T. A. Fuchs, Circulating Extracellular DNA: Cause or Consequence of Thrombosis? *Semin Thromb Hemost* **43**, 553-561 (2017).
33. P. Smith *et al.*, Markers of neutrophil activation and neutrophil extracellular traps in diagnosing patients with acute venous thromboembolism: A feasibility study based on two VTE cohorts. *PLoS One* **17**, e0270865 (2022).
34. J. A. Diaz *et al.*, Plasma DNA is Elevated in Patients with Deep Vein Thrombosis. *J Vasc Surg Venous Lymphat Disord* **1**, (2013).
35. S. Ito *et al.*, A small-molecule compound inhibits a collagen-specific molecular chaperone and could represent a potential remedy for fibrosis. *J Biol Chem* **292**, 20076-20085 (2017).
36. A. Carestia *et al.*, Mediators and molecular pathways involved in the regulation of neutrophil extracellular trap formation mediated by activated platelets. *J Leukoc Biol* **99**, 153-162 (2016).
37. N. Maugeri *et al.*, Activated platelets present high mobility group box 1 to neutrophils, inducing autophagy and promoting the extrusion of neutrophil extracellular traps. *J Thromb Haemost* **12**, 2074-2088 (2014).
38. P. Andre *et al.*, Critical role for Syk in responses to vascular injury. *Blood* **118**, 5000-5010 (2011).
39. L. M. Holbrook *et al.*, Platelets release novel thiol isomerase enzymes which are recruited to the cell surface following activation. *Br J Haematol* **148**, 627-637 (2010).
40. P. A. Randazzo *et al.*, The Arf GTPase-activating protein ASAP1 regulates the actin cytoskeleton. *Proc Natl Acad Sci U S A* **97**, 4011-4016 (2000).
41. S. M. Aunon-Chancellor, J. M. Pattarini, S. Moll, A. Sargsyan, Venous Thrombosis during Spaceflight. *N Engl J Med* **382**, 89-90 (2020).
42. U. Limper *et al.*, The thrombotic risk of spaceflight: has a serious problem been overlooked for more than half of a century? *Eur Heart J* **42**, 97-100 (2021).
43. A. L. Evans *et al.*, Capture, anesthesia, and disturbance of free-ranging brown bears (Ursus arctos) during hibernation. *PLoS One* **7**, e40520 (2012).

44. L. Sachs *et al.*, Ex vivo anticoagulants affect human blood platelet biomechanics with implications for high-throughput functional mechanophenotyping. *Commun Biol* **5**, 86 (2022).
45. J. Krabbe *et al.*, Blood collection technique, anticoagulants and storing temperature have minor effects on the isolation of polymorphonuclear neutrophils. *Sci Rep* **10**, 14646 (2020).
46. N. A. Kulak, G. Pichler, I. Paron, N. Nagaraj, M. Mann, Minimal, encapsulated proteomic-sample processing applied to copy-number estimation in eukaryotic cells. *Nat Methods* **11**, 319-324 (2014).
47. F. Meier *et al.*, Online Parallel Accumulation-Serial Fragmentation (PASEF) with a Novel Trapped Ion Mobility Mass Spectrometer. *Mol Cell Proteomics* **17**, 2534-2545 (2018).
48. P. Skowronek *et al.*, Rapid and In-Depth Coverage of the (Phospho-)Proteome With Deep Libraries and Optimal Window Design for dia-PASEF. *Mol Cell Proteomics* **21**, 100279 (2022).
49. V. Demichev, C. B. Messner, S. I. Vernardis, K. S. Lilley, M. Ralser, DIA-NN: neural networks and interference correction enable deep proteome coverage in high throughput. *Nat Methods* **17**, 41-44 (2020).
50. J. B. Muller-Reif *et al.*, A New Parallel High-Pressure Packing System Enables Rapid Multiplexed Production of Capillary Columns. *Mol Cell Proteomics* **20**, 100082 (2021).
51. J. Cox, M. Mann, MaxQuant enables high peptide identification rates, individualized p.p.b.-range mass accuracies and proteome-wide protein quantification. *Nat Biotechnol* **26**, 1367-1372 (2008).
52. C. Thalin *et al.*, Quantification of citrullinated histones: Development of an improved assay to reliably quantify nucleosomal H3Cit in human plasma. *J Thromb Haemost* **18**, 2732-2743 (2020).
53. A. Pavy-Le Traon, M. Heer, M. V. Narici, J. Rittweger, J. Vernikos, From space to Earth: advances in human physiology from 20 years of bed rest studies (1986-2006). *Eur J Appl Physiol* **101**, 143-194 (2007).
54. S. Tyanova *et al.*, The Perseus computational platform for comprehensive analysis of (prote)omics data. *Nat Methods* **13**, 731-740 (2016).
55. D. B. Bekker-Jensen *et al.*, Rapid and site-specific deep phosphoproteome profiling by data-independent acquisition without the need for spectral libraries. *Nat Commun* **11**, 787 (2020).

Acknowledgments

We thank all members of the Proteomics and Signal Transduction Group and the Clinical Proteomics Group for help and discussions and in particular Igor Paron for technical assistance and Mario Oroshi. We thank Anne Randi Graesli, Michael Lorenz, Inas Saleh and Elisabeth Raatz for excellence technical assistance. Bear captures were led by Sven Brunberg and David Alquist.

Funding

This work was supported by the German Research Foundation (PE2704/2-1 and PE2704/3-1 to TP, SFB 1123-project B06 to S.M., TRR267 – ID 403584255 project B06 to A.D.), by LMU Munich's Institutional Strategy LMU excellent within the framework of the German Excellence Initiative [No. 806 32 006] to T.P., by the DZHK (German Center for Cardiovascular Research) to TP [External collaboration No. 100378833], by the LMU Munich's Clinician scientist program in vascular medicine (PRIME) to M.T and by the LMU Munich's institutional Förderprogramm für Forschung und Lehre (FöFoLe) to M.T. This project has received funding from the European Research Council (ERC) under the European Union's Horizon 2020 research and innovation program (grant agreement No. 833440 to S.M.), The work was also partially supported by the Max Planck Society for the Advancement of Science awarded to MM. The SANS bedrest study was funded by DLR and NASA (contract No 80JSC019P0010 and No 80JSC018P0078). DLR and NASA designed the bed rest study, but had no role in the design, data analysis, manuscript draft, or decision to publish the part of the study described in this manuscript. U.L. received funding from the internal grant program (project IFF 2020-26) of the Faculty of Health at Witten/Herdecke University, Germany, during preparation of this work. JMG and GL received funding from the British Heart Foundation FS/17/31/32848. The Scandinavian brown bear research project is funded by the Norwegian Environment Agency and the Swedish Environmental Protection Agency.

Author contribution

Conceptualization: OF, TP

Methodology: MT, JMR, ZZ, VE, PG, MS, JK, AE, OM, MV, ST, AD, AF, PJ, MMA, AB, MZ, AP, KS, SK, JG, DM, UL, MM, SM

Investigation: MT, JMR, ZZ, VE, JH, KS, BK, LS, JN, EL, GL, MO, LN, SEN, AP, BK, UL

Visualization: ZZ, VE, JMR, MT, KS, AT, SO

Supervision: TP, SM, MM, OF

Writing original draft: MT, JMR, ZZ, MM, TP

Writing review and editing: JMR, MM, SM, MT, TP

Competing interests

The authors declare that they have no competing interests.

Data and material availability

All data are available in the main text, supplementary material or online storage:

The MS-based proteomics data have been deposited to the ProteomeXchange Consortium via the PRIDE partner repository and are available via ProteomeXchange with identifier PXD030465, PXD031521 and PXD039087.

List of Supplementary Materials

Materials and Methods

Figures S1 to S6:

Tables S1 to S6

References (*43-55*)

Figure legends:

Figure 1: Venous thrombosis in brown bears. (A) D-Dimer levels were determined in serially measured plasma from brown bears during active phase and hibernation (n = 15; symbols represent individual bears; data shown as means ± SD; p-values were determined using Wilcoxon test). (**B**) Histological images of organized and re-canalized pulmonary thromboembolism in human and bear lung samples shows neo-vessel lumina (arrows) within organized thrombus (asterisks). Hematoxylin-eosin (H&E), Elastica-van-Giesson. Scale bars indicate 50 µm. (**C**) Representative immunofluorescence images of pulmonary thrombi in human (upper set) and bear lung samples (lower set). Upper sub-panels: red: MPO, green: fibrinogen, blue: 4′,6-diamidino-2-phenylindole (DAPI)). Scale bars indicate 50 µm. The lower sub-panels show a magnification of the thrombus areas with NET structures (green: MPO, blue: 4′,6-diamidino-2-phenylindole (DAPI), red: CitH3 triple positive cells). Scale bars indicate 10 µm. (**D**) Representative H&E picture of bear lung thrombi before and after laser capture microdissection (LCM). Thrombi within vessels (asterisks) were cut out and pooled per individual for MS-based proteomics analysis. (**E**) Comparison of average, mean width adjusted protein intensities from bear and human lung thrombi (n = 3 per organism) cut out from H&E stained FFPE tissue slides with LCM. The proteins with highest intensities (gray), proteins from the coagulation cascade (blue), platelet markers (red), and neutrophile specific elastase (green) are highlighted with gene name**.**

Figure 2: Platelet function in hibernating brown bears.

(A) Field study scheme is shown. (**B**) Quantification of clotting time and mean clot firmness using thromboelastography after INTEM, EXTEM and FIBTEM activation. Differences between blood from summer (n = 8), cool blood from winter (33°C; n = 6) and warmed blood from winter (37°C; n = 8) were analyzed. Symbols represent individual bears; data shown as means ± SD; p-values were determined with one-way Anova test. **(C)** Light transmission aggregometry of washed platelets from winter and summer bears was performed after stimulation with the indicated agonists. Maximum aggregation after 6 minutes was assessed and representative aggregation curves are shown (n = 5 for thrombin 0.01 U/ml and thrombin

0.1 U/ml, n = 4 for collagen 20 µg/ml, n = 7 for collagen 10 µg/ml; symbols represent individual bears; data shown as means ± SD; p-values were determined with paired t-test for collagen 20 µg/ml and thrombin 0.1 U/ml; Wilcoxon test for collagen 10 µg/ml and unpaired t-test for thrombin 0.01 U/ml). (**D)** Secreted proteins from bear platelets (winter and summer) were analyzed upon collagen stimulation or control treatment with MS-based proteomics. Proteins changing significantly (FDR 5 %) in one of the two group comparisons are highlighted in colors and only proteins with a fold-change > 1.5x for the collagen stimulation are shown. Dashed diagonal lines mark the 2x fold-change threshold between x- and y-axis comparison. **(E)** Spreading size of individual platelets stimulated with the indicated agonists on soluble collagen I coated surfaces was analyzed after 8, 15, and 30 minutes (n = 7; symbols represent individual bears; data shown as means ± SD; p-values were determined with paired t-test). Representative images show spreading after 15 minutes; scale bar represents 20 µm. **(F)** Statistical analysis of the platelet proteome of hibernating and active bear platelets reveals HSP47 as the most changed protein (fold-change of 55.26). Changed proteins involved in ROCK1 signaling are marked with gene names. Proteins significantly changing (FDR < 0.05) are highlighted in red in an unpaired analysis of 8 individuals' platelets during hibernation phase and activity. **(G)** Proteomes of bear platelets ranked by mean protein intensity of the 8 individuals for summer and winter. The rank of HSP47 changes from 184 (summer) to 1624 (winter). **(H)** Representative immunoblots of three individual bears during winter and summer for HSP47 in platelets are shown. **(I)** Group expression (MS-based proteomics) of a panel of platelet surface activation markers is shown as violin plots, which reveal an absence of regulation between the summer and winter samples.

Figure 3: Antithrombotic mechanism under HSP47 inhibition.

(A) Scheme of a vena cava thrombosis model. (**B**) Immunoblots for HSP47 in platelets of individual HSP47 knock-out mice and littermate controls are shown. **(C)** Thrombus weight was analyzed after 48 h (n = 10; symbols represent individual mice; data shown as means ± SD; p-values were determined using unpaired t-test). **(D)** NETs in explanted thrombi of HSP47-deficient mice and control animals were analyzed with

confocal microscopy. Scale bar represents 200 µm. Magnifications of thrombus areas with NET structures (MPO- 4′,6-diamidino-2-phenylindole (DAPI) -CitH3 triple positive cells) are shown on the right. Quantitative comparison of NETs per vessel in the HSP47-deficient mice (*PF4-Cre(+)/HSP47*$^{-/-}$) and littermate controls (*PF4-Cre(-)/HSP47*$^{fl/fl}$) is shown as a bar plot on the right (n = 10; data shown as means ± SD; p-values were determined with Mann-Whitney-test). **(E)** Levels of citH3-DNA complexes in paired hibernating and active bears. Dashed line indicates human reference in healthy controls. Supernatant from PMA-stimulated bear neutrophils was used as positive control (n = 4 for winter and summer bears, n = 3 for PMA stimulated neutrophils; symbols represent individual bears; data shown as means ± SD; p-values were determined with paired t-test). **(F)** Quantification of NETs per neutrophil in bears after stimulation of platelets with the indicated agonists (n = 5 per group; data shown as means ± SD; p-values were determined with paired t-test for thrombin, collagen, and PMA; Wilcoxon test was used for unstimulated). Scale bar represents 50 µm; magnification of NET structure is shown on the left. (**G**) In vitro formation of human PMN-platelet aggregates in the presence or absence of HSP47 inhibitor Col003 (SMI I) after platelet stimulation with the indicated agonists. Representative flow-cytometric contour plots are shown (n = 4; symbols represent independent experiments; data shown as means ± SD; p-values were determined using paired t-test). (**H**) NET formation was analyzed using confocal microscopy following in vitro co-culture of human neutrophils and platelets after stimulation with the indicated agonists following HSP47 inhibition (SM I; symbols represent independent experiments; data shown as means ± SD; p-values were determined using Wilcoxon test for unstimulated and paired t-test for collagen and thrombin). Scale bar represents 5 µm.

Figure 4: HSP47 regulates thromboinflammation. (A) Multi-color flow cytometry on platelets following activation with indicated stimuli in the presence or absence of HSP47 inhibitor (SMI I) is shown. T-Distributed Stochastic Neighbor Embedding (t-SNE) of platelet heterogeneity is displayed by Flow-SOM plots. Heatmap of the mean fluorescence intensity (MFI) for each platelet subcluster relative to the maximum MFI of the surface marker is shown. Frequency of population 5 following SMI I or vehicle

treatment is shown (n = 4; bars show means ± SD; p-values were determined using paired t-test). **(B)** Changing peptides from phospho-proteome analysis of activated platelets under SMI I treatment compared to vehicle treatment after collagen/thrombin stimulation. The phospho-proteome of 6 individuals was compared by independent t-test and average fold changes of all peptides are displayed in the histograms. **(C)** Thrombin binding to the surface of platelets from healthy control patients was analyzed using flow cytometry after addition of two different HSP47 small molecule inhibitors (n = 5 for SMI I (Col003), n = 4 for SMI II (RH00007SC). Symbols represent individuals; data shown as means ± SD; p-values were determined using paired t-test. (**D**) Thrombin binding to the surface of platelets from HSP47-deficient mice (*PF4-Cre(+)/HSP47*$^{-/-}$) and littermate controls (*PF4-Cre(-)/HSP47*$^{fl/fl}$) was examined. Symbols represent individuals; data shown as means ± SD; p-values were determined using unpaired t-test. (**E**) ROS production and **(F)** CD11b surface expression on neutrophils upon stimulation with purified HSP47 peptide and fMLP. Bars show means ± SD; symbols represent individual experiments, n = 4; p-values were determined using paired t-test. **(G)** Percentage of NET-forming neutrophils was analyzed after stimulation with HSP47 peptide or co-stimulation with fMLP and HSP47 peptide (n = 4; bars show means ± SD; p-values were determined using paired t-test). Scale bar represents 30 μm. **(H)** Expression of CD11b (MFI ratio to unstimulated) in neutrophils upon stimulation with the indicated agonists in presence or absence of TLR2 inhibitor. Bars show means ± SD; symbols represent individual experiments, n = 4; p-values were determined using paired t-test. (**I**) Expression of CD11b (MFI ratio to unstimulated) in neutrophils upon stimulation with the indicated agonists in presence or absence of TLR4 inhibitor. Bars show means ± SD; symbols represent individual experiments, n = 4; p-values were determined using multiple t-test. (**J**) CD11b surface expression (MFI ratio to unstimulated) in neutrophils upon stimulation with the indicated agonists in presence or absence of MyD88 inhibitor. Bars show means ± SD; symbols represent individual experiments, n = 5 for unstimulated and HSP47; n = 4 for LPS and fMLP; p-values were determined using paired t-test.

Figure 5: Thrombus protection by HSP47 downregulation.

(A) Schematic view of the recruited SCI cohort and healthy controls. **(B)** Platelet expression of HSP47 (MFI) in healthy controls and patients with SCI. Representative flow cytometry histograms are shown (n = 19; data shown as means ± SD; p-values were determined using Mann-Whitney test). **(C)** Representative immunoblot for HSP47 in human platelets from immobile patients and matched healthy controls. **(D)** Immunofluorescence microscopy of HSP47 (red) and actin (green) was performed in platelets from patients with SCI and healthy controls. HSP47 fluorescence intensity was quantified (violin plot shows median (thick dotted line) and interquartile range (thin dotted lines); cells from 3 independent experiments were analyzed). Representative cells are shown in both profile and histogram (MFI). Scale bar indicates 10 μm; p-values were determined using Mann-Whitney test. (**E**) Thrombin binding was analyzed using flow cytometry in patients with SCI (n = 8 for patients with SCI and healthy controls. Symbols represent individual humans; data shown as means ± SD; p-values were determined using Mann-Whitney test. Representative flow cytometry is shown). **(F)** Quantification of platelet activation marker expression (MFI ratios to unstimulated) by flow cytometry following stimulation with the indicated agonists (bars represent means ± SD; symbols represent single SCI patients or healthy controls; n = 8 per group; p-values were determined using unpaired t-test for p-selectin stimulation with thrombin, PAC-1, CD63; Mann-Whitney was used for p-selectin stimulation with collagen). **(G)** Quantification of platelet-PMN aggregates following platelet stimulation with thrombin. Representative flow-cytometric contour plots from 8 independent experiments are shown. **(H)** Quantification of human PMN-platelet aggregates formation after platelet stimulation with thrombin in vitro (symbols represent individual SCI patients and healthy controls n = 8 per group; bars show mean ± SD: p-values were determined using unpaired t-test). **(I)** Quantification of NETs per neutrophil after stimulation of platelets with indicated agonists (bars represent means ± SD; symbols represent single patients or healthy controls; n = 8 per group; p-values were determined using unpaired t-test). **(J)** Pooled (patients and healthy controls; n = 16) correlation analysis of HSP47 expression with thrombin induced aggregates or thrombin-induced NETs, given as r^2-values; analysis was done using

Pearson correlation. (**K**) *HSP47* mRNA was quantified in platelets from patients with SCI and healthy controls (n = 4). Bars represent means ± SD; symbols represent single patients or healthy controls; p-values were determined using Mann-Whitney test. **(L)** Schematic view of the bed rest cohort analyzed. **(M)** Serial analysis of HSP47 expression at indicated time points is shown (symbols represent single individuals; n = 10 per group; p-values were determined using Wilcoxon test). (**N**) Correlation of protein fold changes from proteomics analysis of the hibernating vs. active bears and human individuals before and after 27 days of bedrest. Proteins with a t-test p-value < 0.05 in one of the two sets are highlighted in red. Proteins in the upper right quadrant are co-downregulated in bears and humans upon immobility (e.g. HSP47, SYK, ASAP1), whereas proteins in the bottom left quadrant are co-upregulated upon immobility**.** (**O**) Platelet expression of HSP47 (MFI) in immobile and mobile pigs (n = 5; symbols represent individual pigs; data shown as means ± SD; p-values were determined using unpaired t-test). Representative flow cytometry histograms are shown.

Figure 1

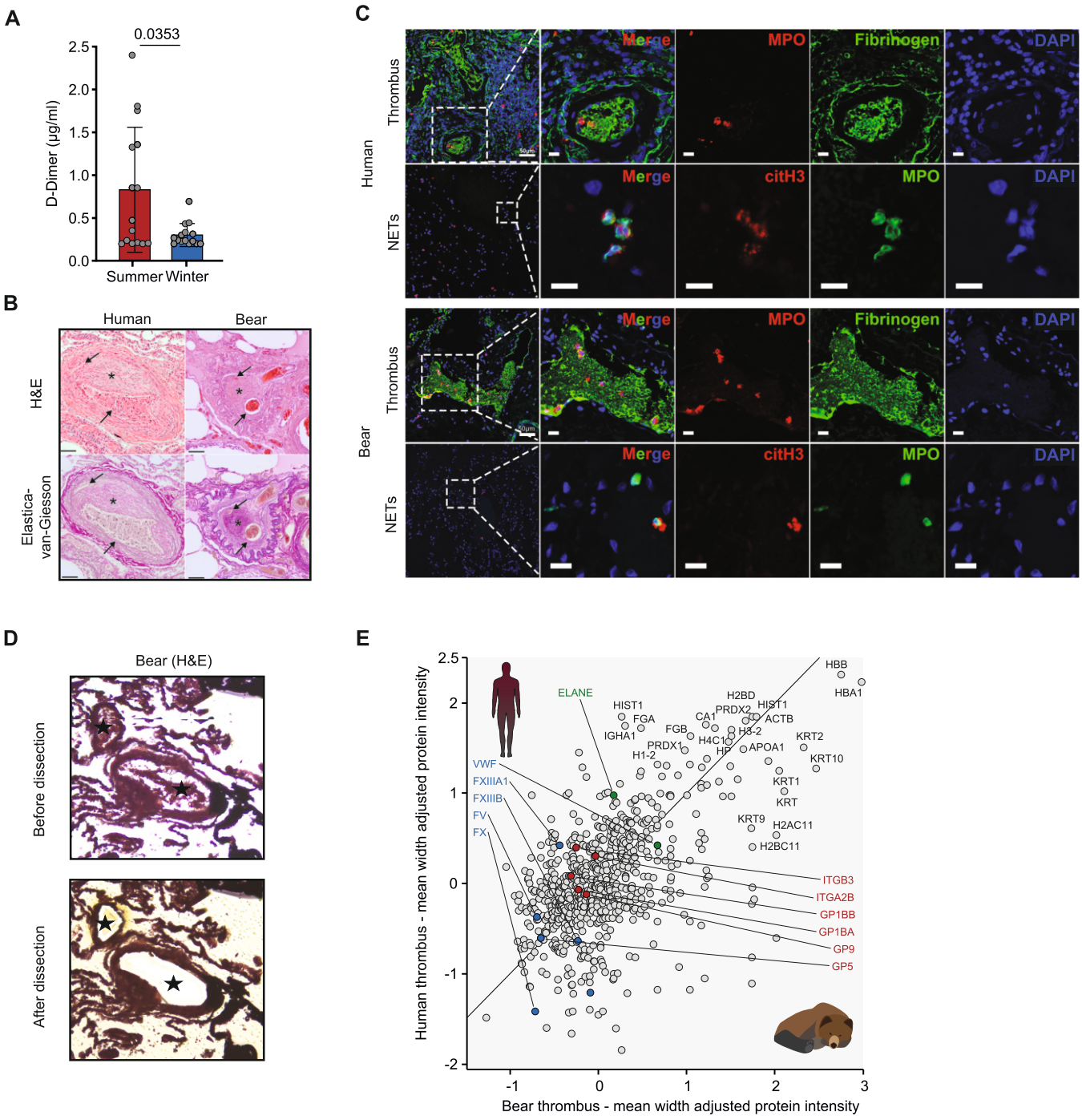
A
0.0353
D-Dimer (µg/ml)
Summer
Winter
B
Human
Bear
H&E
Elastica-van-Giesson
C
Thrombus
NETs
Human
Bear
Merge
MPO
Fibrinogen
DAPI
citH3
D
Bear (H&E)
Before dissection
After dissection
E
Human thrombus - mean width adjusted protein intensity
Bear thrombus - mean width adjusted protein intensity
ELANE
HBB
HBA1
HIST1
FGA
IGHA1
FGB
CA1
PRDX2
H2BD
ACTB
H3-2
PRDX1
H4C1
H1-2
HP
APOA1
KRT2
KRT10
KRT1
KRT
KRT9
H2AC11
H2BC11
VWF
FXIIIA1
FXIIIB
FV
FX
ITGB3
ITGA2B
GP1BB
GP1BA
GP9
GP5

Figure 2

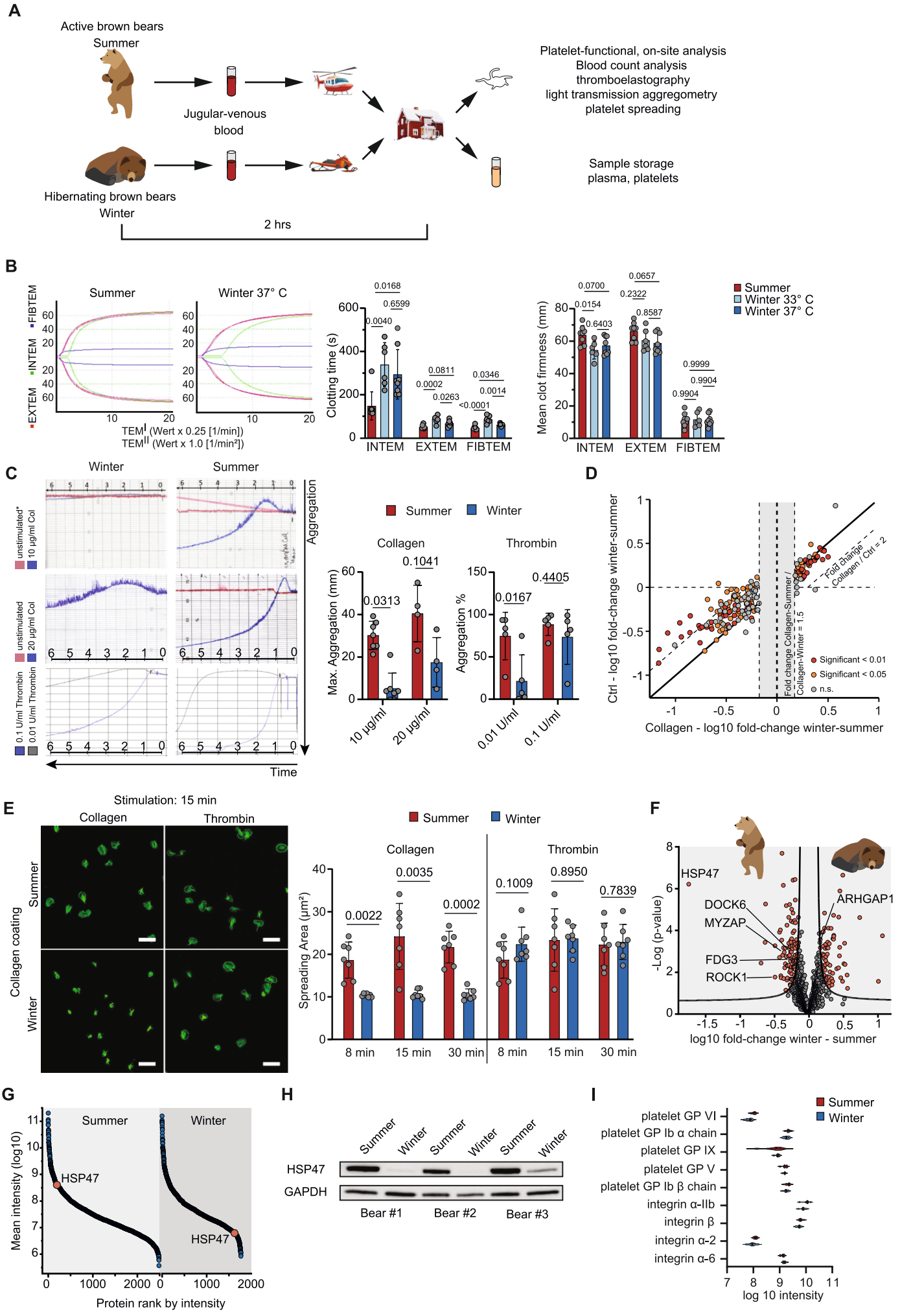
A
Active brown bears
Summer
Jugular-venous
blood
Hibernating brown bears
Winter
2 hrs
Platelet-functional, on-site analysis
Blood count analysis
thromboelastography
light transmission aggregometry
platelet spreading
Sample storage
plasma, platelets
B
Summer
Winter 37° C
FIBTEM
INTEM
EXTEM
TEM I (Wert x 0.25 [1/min])
TEM II (Wert x 1.0 [1/min²])
Clotting time (s)
Mean clot firmness (mm)
INTEM
EXTEM
FIBTEM
Summer
Winter 33° C
Winter 37° C
C
Winter
Summer
unstimulated
10 µg/ml Col
20 µg/ml Col
0.1 U/ml Thrombin
0.01 U/ml Thrombin
Aggregation
Time
Summer
Winter
Collagen
Thrombin
Max. Aggregation (mm)
Aggregation %
10 µg/ml
20 µg/ml
0.01 U/ml
0.1 U/ml
D
Ctrl - log10 fold-change winter-summer
Collagen - log10 fold-change winter-summer
Fold change Collagen-Summer / Collagen-Winter = 1.5
Fold change Collagen / Ctrl = 2
Significant < 0.01
Significant < 0.05
n.s.
E
Stimulation: 15 min
Collagen
Thrombin
Collagen coating
Summer
Winter
Spreading Area (µm²)
8 min
15 min
30 min
F
HSP47
DOCK6
MYZAP
FDG3
ROCK1
ARHGAP1
-Log (p-value)
log10 fold-change winter - summer
G
Summer
Winter
HSP47
Mean intensity (log10)
Protein rank by intensity
H
HSP47
GAPDH
Bear #1
Bear #2
Bear #3
I
platelet GP VI
platelet GP Ib α chain
platelet GP IX
platelet GP V
platelet GP Ib β chain
integrin α-IIb
integrin β
integrin α-2
integrin α-6
log 10 intensity

Figure 3

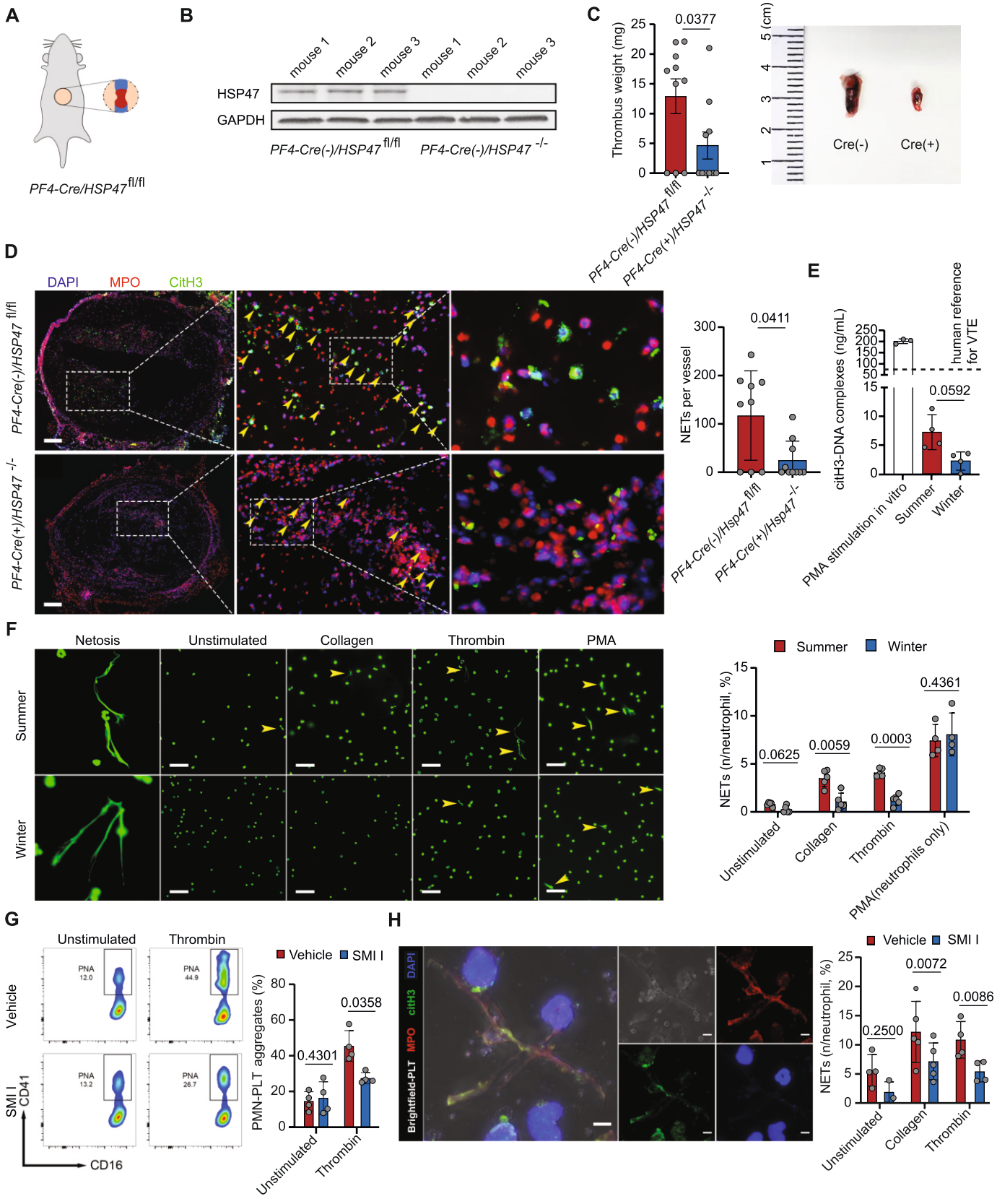
A
PF4-Cre/HSP47fl/fl
B
mouse 1
mouse 2
mouse 3
mouse 1
mouse 2
mouse 3
HSP47
GAPDH
PF4-Cre(-)/HSP47fl/fl
PF4-Cre(-)/HSP47-/-
C
Thrombus weight (mg)
0.0377
PF4-Cre(-)/HSP47fl/fl
PF4-Cre(+)/HSP47-/-
5 (cm)
Cre(-)
Cre(+)
D
DAPI
MPO
CitH3
PF4-Cre(-)/HSP47fl/fl
PF4-Cre(+)/HSP47-/-
E
NETs per vessel
0.0411
PF4-Cre(-)/Hsp47fl/fl
PF4-Cre(+)/Hsp47-/-
citH3-DNA complexes (ng/mL)
human reference for VTE
0.0592
PMA stimulation in vitro
Summer
Winter
F
Netosis
Unstimulated
Collagen
Thrombin
PMA
Summer
Winter
Summer
Winter
NETs (n/neutrophil, %)
0.0625
0.0059
0.0003
0.4361
Unstimulated
Collagen
Thrombin
PMA(neutrophils only)
G
Unstimulated
Thrombin
Vehicle
SMI I
PNA
12.0
PNA
44.9
PNA
13.2
PNA
26.7
CD41
CD16
Vehicle
SMI I
PMN-PLT aggregates (%)
0.4301
0.0358
Unstimulated
Thrombin
H
DAPI
citH3
MPO
Brighfield-PLT
Vehicle
SMI I
NETs (n/neutrophil, %)
0.2500
0.0072
0.0086
Unstimulated
Collagen
Thrombin

Figure 4

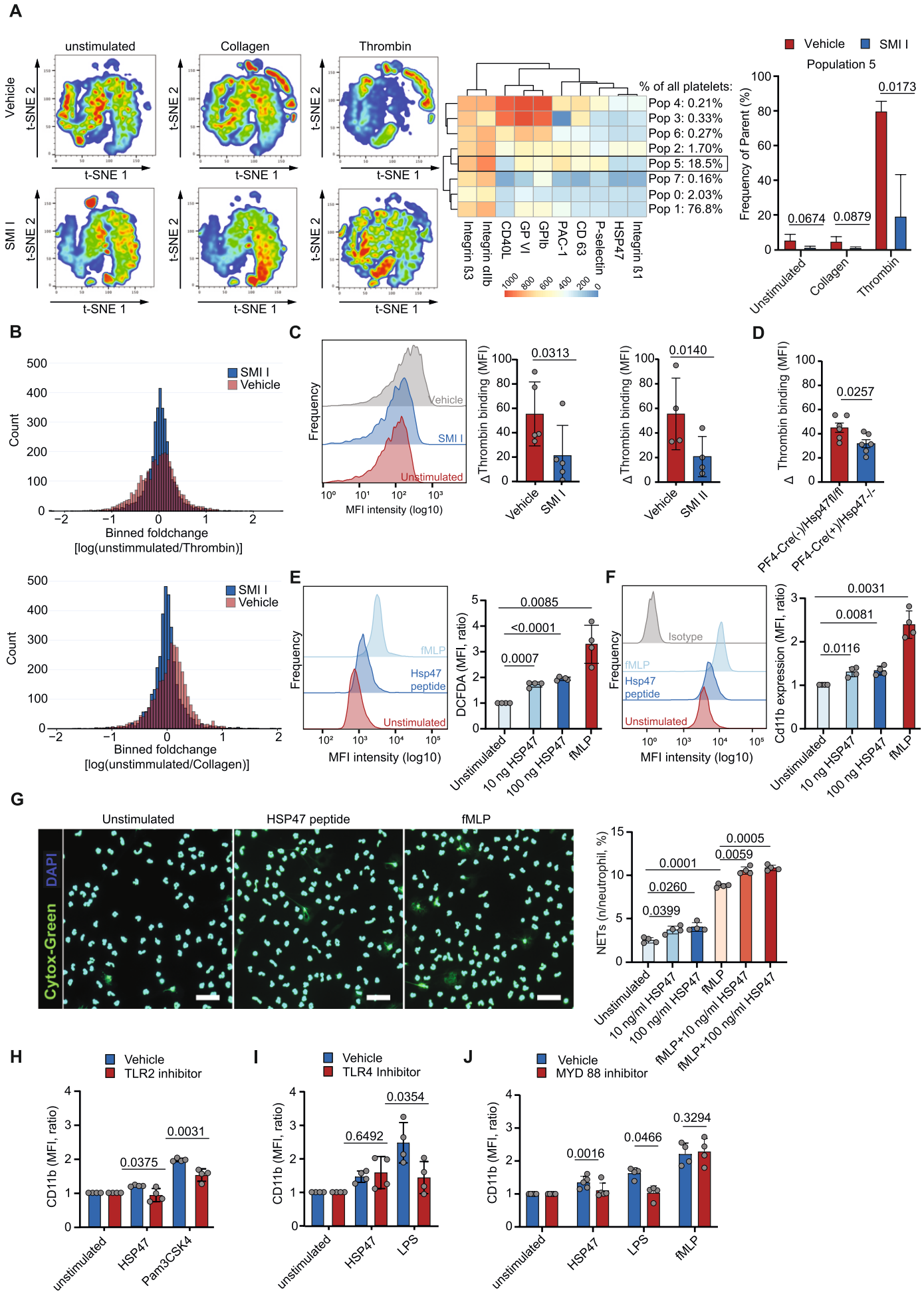
A
unstimulated
Collagen
Thrombin
Vehicle
SMI I
t-SNE 1
t-SNE 2
% of all platelets:
Pop 4: 0.21%
Pop 3: 0.33%
Pop 6: 0.27%
Pop 2: 1.70%
Pop 5: 18.5%
Pop 7: 0.16%
Pop 0: 2.03%
Pop 1: 76.8%
Integrin β3
Integrin αIIb
CD40L
GP VI
GPIb
PAC-1
CD 63
P-selectin
HSP47
Integrin β1
Population 5
Frequency of Parent (%)
0.0674
0.0879
0.0173
Unstimulated
Collagen
Thrombin
B
Count
Binned foldchange
[log(unstimmulated/Thrombin)]
[log(unstimmulated/Collagen)]
C
Frequency
MFI intensity (log10)
Δ Thrombin binding (MFI)
0.0313
0.0140
SMI II
D
0.0257
PF4-Cre(-)/Hsp47fl/fl
PF4-Cre(+)/Hsp47-/-
E
fMLP
Hsp47 peptide
DCFDA (MFI, ratio)
0.0085
<0.0001
0.0007
10 ng HSP47
100 ng HSP47
F
Isotype
Cd11b expression (MFI, ratio)
0.0031
0.0081
0.0116
G
Unstimulated
HSP47 peptide
fMLP
DAPI
Cytox-Green
NETs (n/neutrophil, %)
0.0005
0.0059
0.0001
0.0260
0.0399
10 ng/ml HSP47
100 ng/ml HSP47
fMLP+10 ng/ml HSP47
fMLP+100 ng/ml HSP47
H
TLR2 inhibitor
CD11b (MFI, ratio)
0.0031
0.0375
unstimulated
HSP47
Pam3CSK4
I
TLR4 Inhibitor
0.0354
0.6492
LPS
J
MYD 88 inhibitor
0.3294
0.0466
0.0016
fMLP

Figure 5

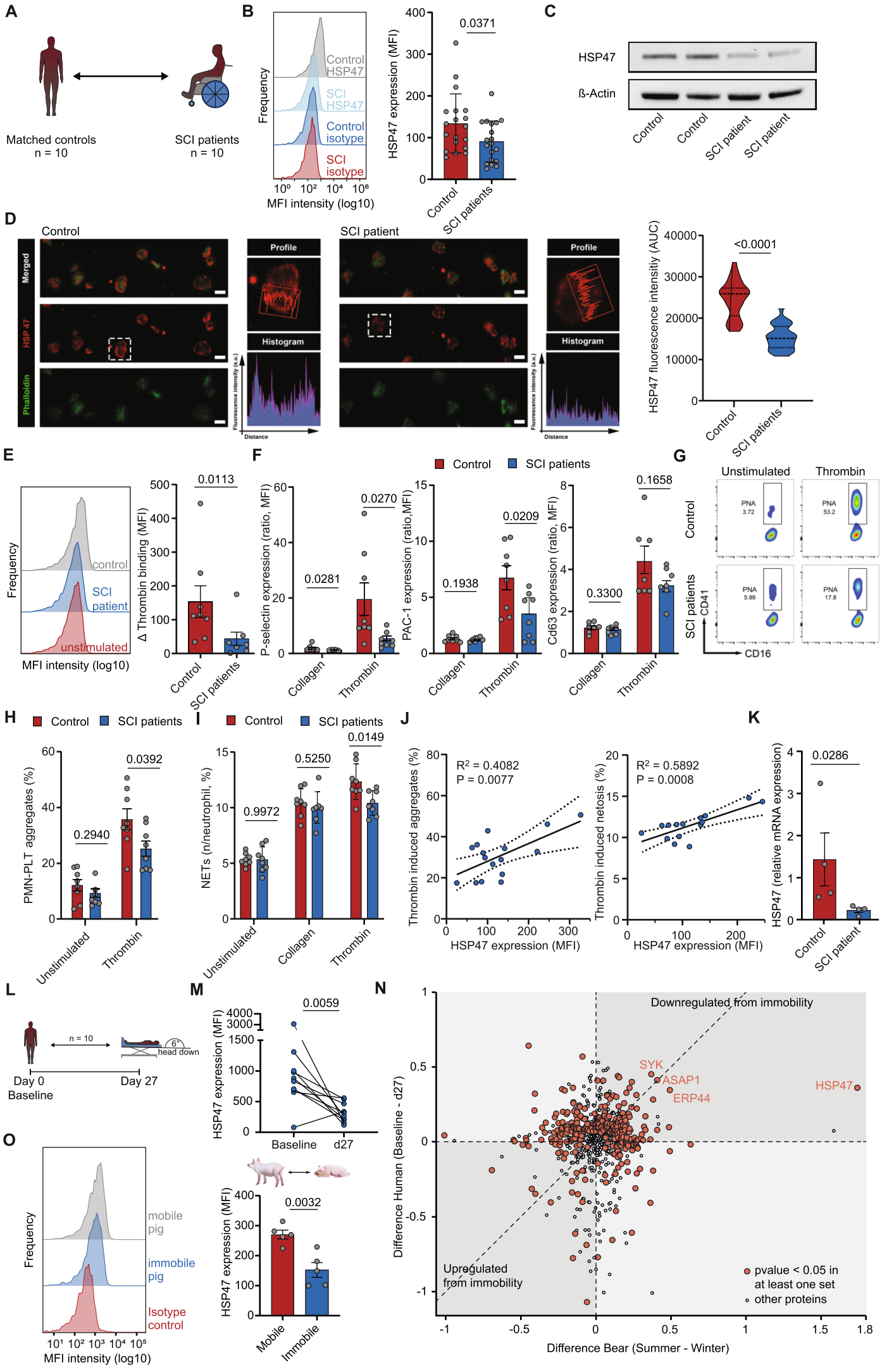
A
Matched controls
n = 10
SCI patients
n = 10
B
Frequency
Control HSP47
SCI HSP47
Control isotype
SCI isotype
MFI intensity (log10)
HSP47 expression (MFI)
0.0371
Control
SCI patients
C
HSP47
ß-Actin
Control
Control
SCI patient
SCI patient
D
Control
SCI patient
Merged
HSP 47
Phalloidin
Profile
Histogram
Fluorescence intensity (a.u.)
Distance
HSP47 fluorescence intensity (AUC)
<0.0001
Control
SCI patients
E
Frequency
control
SCI patient
unstimulated
MFI intensity (log10)
Δ Thrombin binding (MFI)
0.0113
Control
SCI patients
F
Control
SCI patients
P-selectin expression (ratio, MFI)
0.0281
0.0270
Collagen
Thrombin
PAC-1 expression (ratio,MFI)
0.1938
0.0209
Collagen
Thrombin
Cd63 expression (ratio, MFI)
0.3300
0.1658
Collagen
Thrombin
G
Unstimulated
Thrombin
Control
SCI patients
PNA
3.72
PNA
53.2
PNA
5.99
PNA
17.8
CD41
CD16
H
Control
SCI patients
PMN-PLT aggregates (%)
0.2940
0.0392
Unstimulated
Thrombin
I
Control
SCI patients
NETs (n/neutrophil, %)
0.9972
0.5250
0.0149
Unstimulated
Collagen
Thrombin
J
Thrombin induced aggregates (%)
R² = 0.4082
P = 0.0077
HSP47 expression (MFI)
Thrombin induced netosis (%)
R² = 0.5892
P = 0.0008
HSP47 expression (MFI)
K
HSP47 (relative mRNA expression)
0.0286
Control
SCI patient
L
n = 10
6°
head down
Day 0
Baseline
Day 27
M
HSP47 expression (MFI)
0.0059
Baseline
d27
0.0032
Mobile
Immobile
N
Downregulated from immobility
SYK
ASAP1
ERP44
HSP47
Upregulated
from immobility
pvalue < 0.05 in
at least one set
other proteins
Difference Human (Baseline - d27)
Difference Bear (Summer - Winter)
O
Frequency
mobile
pig
immobile
pig
Isotype
control
MFI intensity (log10)

Science
AAAS

Supplementary Materials for

Immobility-associated thromboprotection is conserved across mammalian species from bear to human

Manuela Thienel*[1,2], Johannes B. Müller-Reif*[3,4], Zhe Zhang*[1], Vincent Ehreiser[1,2], Judith Huth[1,2], Khrystyna Shchurovska[1,2], Badr Kilani[1,2], Lisa Schweizer[3], Philipp E. Geyer[3,4], Maximilian Zwiebel[3], Julia Novotny[1], Enzo Lüsebrink[1], Gemma Little[5], Martin Orban[1], Leo Nicolai[1,2], Shaza El Nemr[1,2], Anna Titova[1,2], Michael Spannagl[6], Jonas Kindberg[7,8], Alina L. Evans[9], Orpheus Mach[10], Matthias Vogel[10], Steffen Tiedt[11], Steffen Ormanns[12], Barbara Kessler[13], Anne Dueck[2,14], Andrea Friebe[7,8], Peter Godsk Jørgensen[15], Monir Majzoub-Altweck[16], Andreas Blutke[16], Amin Polzin[17], Konstantin Stark[1,2], Stefan Kääb[1,2], Doris Maier[10], Jonathan M Gibbins[5], Ulrich Limper[18,19], Ole Frobert[20, 21, 22, 23,#], Matthias Mann[3,#], Steffen Massberg[1,2,#], Tobias Petzold[1,2#]

Corresponding authors:

tobias.petzold@med.uni-muenchen.de

steffen.massberg@med.uni-muenchen.de

mmann@biochem.mpg.de

ole.frobert@regionorebrolan.se

The PDF file includes:

Materials and Methods

Figs. S1 to S6

Tables S1 to S6

References (*43-55*)

Materials and Methods

Reagents

All used commercial reagents and antibodies are listed in table S6.

Bear capture and blood draining

Blood samples were collected from 13 free-ranging brown bears (Ursus arctos; mean age 2.4 years; 4 male and 9 female bears) during hibernation (February/March 2019 and 2022) and again from the same bears during their active period in summer (June 2019 and 2022). All bears were previously fitted with global positioning system (GPS) collars and very high frequency (VHF) transmitters as part of the Scandinavian Brown Bear Research Project (https://bearproject.info/) which allowed us to locate the bears in their dens during hibernation and in their habitat during the active state, where they were captured according to established protocols. During winter captures, bears were located in their dens and anesthetized with a mixture of medetomidine, zolazepam, tiletamine, and ketamine. During summer captures, the same bears were darted from a helicopter with a mixture of medetomidine, zolazepam, and tiletamine (*43*). Blood was drawn from the jugular vein and samples were collected in 0.1 M sodium citrate tubes, EDTA tubes, or serum tubes with clotting activator (S-Monovette®, Sarstedt, Germany). According to the requirements of the performed assay, different blood anticoagulants were used that may impact platelets (*44, 45*). However, to allow comparability between immobile and active conditions the same anticoagulant was used for each assay across species. Samples were either immediately analyzed in a field station in Sweden or conserved for subsequent elaborative analysis in Munich. For plasma analysis of circulating DNA level and D-dimer level, citrate plasma samples from earlier bear capture were included in analysis. The study was approved by the Swedish Ethical Committee on Animal Research (C18/15 and C3/16), and the procedures were performed in compliance with Swedish laws and regulations.

Recruitment of patients with SCI and blood sampling

The study conformed to the 1975 Declaration of Helsinki and was approved by the Ethics Committee of the Ludwig-Maximilians-University Munich. In an open, prospective design, chronically immobile patients in stable disease state (≥12 months) after disabling spinal cord injury (SCI) and healthy controls matched for age, sex, and antithrombotic therapy were recruited at the Berufsgenossenschaftliche Unfallklinik Murnau and LMU hospital, respectively. Exclusion criteria were known hematological disorders, active hematological malignancy, severe renal insufficiency with dialysis, age below 18 years, and no informed consent. As we recruited patients who experienced disabling spinal cord injury at least 12 months ago (except of one patient, who was included after 9 months), we do not have baseline HSP47 level before injury, which is a limitation of this study. Blood from patients and healthy individuals was obtained after written informed consent by venous puncture from a dorsum manus or cubital vein. A 21 G butterfly needle (Safety-Multifly®-Needle, Sarstedt, Germany) was used. Samples were collected in 2.9 ml 0.1 M sodium citrate tubes, 7.5 ml lithium-heparin tubes, 2.6 ml EDTA tubes, or 4.5 ml serum tubes with clotting activator (S-Monovette®, Sarstedt, Germany). Blood was transferred to LMU hospital for further analysis. Given organizational constraints, not all experiments could be performed in all patients. Experiments were performed within 2 h after blood sampling. According to the requirements of the performed assay, different blood anticoagulants were used that may impact platelet and neutrophil function (*44, 45*). However, to allow comparability between immobile and active conditions the same anticoagulant was used for each assay across species.

Recruitment of acutely immobile patients and blood sampling

The study conformed to the 1975 Declaration of Helsinki and was approved by the Ethics Committee of the Ludwig-Maximilians-University Munich. In an open, prospective design, acutely immobile patients after intracerebral bleeding were recruited at the LMU hospital. Exclusion criteria were known hematological disorders, active hematological malignancy, severe renal insufficiency with dialysis, age below 18 years. Blood from patients was obtained by venous puncture from a dorsum manus or cubital vein. A 21 G butterfly needle (Safety-Multifly®-Needle, Sarstedt, Germany) was used. Samples were collected in 2.9 ml 0.1 M sodium citrate tubes and 2.6 ml EDTA tubes (S-Monovette®, Sarstedt, Germany). According to the requirements of the performed assay, different blood anticoagulants were used that may impact platelet and neutrophil function (*44, 45*). However, to allow comparability between immobile and active conditions the same anticoagulant was used for each assay across species.

Blood sampling in immobile pigs

Blood was drawn from free-ranging and mobility-limited pigs (Sus scrofa domesticus) in cooperation with the Gene Center of the Ludwig-Maximilians-University Munich. All animal experiments were performed with approval by the Government of Bavaria (Munich, Germany). A few days before giving birth to their piglets, breeding sows were confined in farrowing crates (width: 55 – 70 cm, length: 140 – 170 cm) which allow only very limited mobility and thus prevent the sows from squashing their offspring. 3-4 weeks after birth and limited mobility in the farrowing crates pigs were defined as immobile and blood was drawn from the jugular vein. Samples were collected in 0.1 M sodium citrate tubes. Mobile pigs were neither breeding nor gave birth within the last weeks which is a limiting factor, as changes in coagulation status occur during pregnancy and lactation potentially involving alterations in HSP47 expression. Moreover, we have not performed further functional measurements of porcine blood cells.

Histology

To analyze the presence of venous pulmonary emboli in brown bears, we examined pulmonary samples taken from brown bears deceased in zoo husbandry between 1994 and 2018 and provided by the veterinary faculty of Ludwig-Maximilians-University Munich. Based on the pathological sections, hematoxylin-eosin stains (H&E), Elastica-van-Giesson stains as well as immunofluorescence stains were prepared. Patients with clinically diagnosed and histologically confirmed pulmonary artery embolism served as a known comparative population. The study conformed to the 1975 Declaration of Helsinki and was approved by the Ethics Committee of the Ludwig-Maximilians-University Munich. Immunofluorescent stains were prepared using a triple stain against myeloperoxidase (MPO, R&D Systems, US), citrullinated histone 3 (rabbit polyclonal to Histone H3, Abcam, Germany), and Hoechst (1:1000, Invitrogen, US) or a triple stain against myeloperoxidase, fibrinogen (rabbit anti-human, A0080 Dako, US), and Hoechst. NETing neutrophils were designated as such when a triple positive staining occurred.

LCM and Sample Preparation

FFPE tissue sections (thickness: 5 µm) derived from three human and three bear specimens were prepared and stained by H&E as described earlier. Thrombi in the respective sample were extracted using Laser Capture Microdissection (LCM) on a Leica LMD7 instrument. Dissected tissue was collected in caps of 0.2 mL tubes and subsequently transferred to a 96-well plate (96 AFA-TUBE TPX Plate, Covaris) by centrifugation for 2 min at 1000 × g. Samples were lysed

by consecutive heating at 90° C for 10 min and 80 min, interrupted by focused sonification (LE220-plus Covaris Focused-ultrasonicator; duration: 300 s, peak power: 450.0, duty factor: 50 %, cycles: 200, average power: 225) in lysis buffer (300 mM Tris, 5 mM TCEP and 25 mM CAA final concentration). Enzymatic protein digest was performed by adding 0.5 µg LysC for 4 h and was complemented by 0.5 µg of trypsin overnight at 37° C and 1200 rpm. Thereafter, the reaction was quenched by the addition of TFA to a final concentration of 1 %. The resulting peptides were purified using the iST protocol *(46)*. In brief, 20 µg of peptides were loaded onto in-house generate SDB-RPS (Empore™ SPE Disks, CDS Analytical, 98-0604-0226-4) tips by centrifugation, followed by consecutive washing steps using 1 % TFA in isopropanol and 0.2% TFA in MS-grade H_2O, respectively. Peptides were eluted using 80 % AcN, 1 % NH4+ in MS-grade H_2O, dried using a SpeedVac centrifuge at 45° C (Eppendorf, Concentrator Plus) and resuspended 2 % acetonitrile (v/v) and 0.1 % trifluoroacetic acid (v/v) in MS-grade H_2O.

Mass Spectrometry for LCM

Liquid chromatography-mass spectrometry (LC-MS) was performed on an EASY-nLC 1200 ultrahigh-pressure system (Thermo Fisher Scientific)) coupled to a hybrid TIMS quadrupole TOF mass spectrometer (timsTOF Pro, Bruker) via a CaptiveSpray nano-electrospray ion source. For the MS data acquisition, 200 ng of peptides were separated on an in-house packed column (50 cm, inner diameter: 75 µm, generated in-house using ReproSil-Pur C18-AQ 1.9 µm beads [Dr. Maisch GmbH]) for a gradient length of 120 min. To provide a gradual elution of peptides injected in buffer A (0.1% FA in H_2O), the percentage of buffer B (80 % acetonitrile, 0.1 % FA in H_2O) was increased from 3 % to 30 % within 95 min, followed by an increase to 60 % within 5 min and a constant level of 95 % for further 5 min. The flow rate was set to 300 nl/min.

MS data were recorded using a data-independent acquisition method that is embedded in parallel accumulation–serial fragmentation (*47, 48*). This dia-PASEF method covered an m/z-range from 350 to 1200 in 12 isolation windows (cycle time: 1.4 s). The isolation width varies since it is optimized for the precursor distribution in the m/z and ion mobility dimension. Ion mobility values were covered from 1/K0 = 1.3 Vs cm-2 to 0.7 Vs cm-2 using TIMS ramp times of 100 ms. For MS2 scans, the m/z-range was set from 100 to 1,700 and collision energies were defined linearly to the ion mobility from 59 eV at 1/K0=1.6 Vs cm−2 to 20 eV at 1/K0=0.6 Vs cm−2. MS data acquisition was performed on the tims control software (version 3.0.20, Bruker Daltonik GmbH).

MS data were processed in the DIA-NN software version 1.8.1 (*49*) as described earlier. Setting details have been deposited to the ProteomeXchange Consortium via the PRIDE partner repository and are available via ProteomeXchange with identifier and PXD039087.

Mouse work

HSP47$^{fl/fl}$ mice were kindly provided by Kazuhiro Nagata and breed with *PF4-Cre* mice to generate *PF4-Cre /HSP47*$^{fl/fl.}$ mice Bone marrow chimeras were generated by injecting 10x106 bone marrow cells isolated from *PF4-Cre(+)/HSP47*$^{-/-}$ or *PF4-Cre(-)/HSP47*$^{fl/fl}$ littermate controls into the tail vein of sublethal irradiated 8-week-old female CD45.1 wildtype mice. Six weeks after bone marrow transplantation, blood counts were analyzed on a hematology system blood counter (Sysmex, Japan). Chimerism was determined by analyzing the percentage of CD45.2+ positive cells in the CD45+ population in peripheral blood using flow cytometry. Flow cytometry was done using BD Canto 2 (BD Biosciences, US) following incubation with labelling antibodies and fluorescent bead calibration. All animal experiments were performed with approval by the Government of Bavaria (Munich, Germany) or in accordance with a license from the UK Home Office.

Mouse model of deep vein thrombosis

Flow reduction in the inferior vena cava (IVC) was achieved as described *(3)* without ligation of side branches, and thrombi were harvested after 48 h. Sex, age, and weight-matched groups were used for analysis. Analysis was done in a blinded manner regarding group. Animals with bleeding from the IVC were excluded from further analysis. Although the frequency of thrombus occurrence (60-80 %) and its variability is a notable limitation of this model, it mimics human DVT more closely than other models triggered by chemical or physical vessel damage as thrombus formation occurs over several days without the induction of major vascular damage.

Murine platelet isolation

Blood was drained by cardiac puncture in anesthetized mice. Citrated blood was diluted 1:3 in Tyrode's Buffer (137 mM NaCl, 2.8 mM KCl, 12 mM $NaHCO_3$, 5.5 mM glucose, 10 mM HEPES, pH = 6.5) and centrifuged at 70 × g for 20 min at room temperature (RT). Platelet rich plasma (PRP) was further diluted with Tyrode's Buffer and centrifuged at 600 × g for 10 min at RT. For further analysis the platelet pellets were re-suspended in Tyrode's Buffer (pH=7.4).

Platelet isolation in humans, bears, and pigs

Citrate anticoagulated blood was centrifuged with 90 × g for 20 min at RT. PRP was then diluted 1:10 in modified Tyrode's buffer (137 mM NaCl, 2.8 mM KCl, 12 mM $NaHCO_3$, 5.5 mM glucose, 10 mM HEPES, pH = 6.5) substituted with prostaglandine (PGI_2, 500 ng/ml final concentration, Abcam, Germany). PRP was centrifuged at 450 × g for 10 min at RT. Cells were re-suspended in Tyrode's buffer (pH = 7.4). For proteome analysis, platelets were purified using a magnetic activated cell sorting (MACS) based negative isolation kit. Platelet suspension was incubated with glycophorin A MicroBeads (130-050-501, MACS Miltenyi Biotec, Germany) and CD45 MicroBeads (MACS Miltenyi Biotec) before running over a LS Column (MACS Miltenyi Biotec). Cells were pelleted at 2,500 × g for 5 min, resuspended in lysis buffer (preOmics, Germany) and immediately frozen in liquid nitrogen. Platelet-poor plasma (PPP) was obtained by centrifugation.

Human neutrophil isolation

Neutrophils were isolated from whole blood using the MACS neutrophil isolation kit (Miltenyi Biotec, Germany). Briefly, whole blood was incubated with MACS negative selection antibody panel and subsequently inserted into a magnet in a FACS tube (StemCell Technologies, USA). The supernatant was collected, then centrifuged at 350 × g for 7 min at 4° C and the erythrocytes were consequently removed by addition of erylysis buffer (155 mM NH_4Cl_2, 10mM $KHCO_3$, 0.1 mM EDTA, pH 7.3). Lysis was stopped after 10 min by addition of phosphate buffered saline (PBS) containing 2 mM EDTA. Isolated neutrophils were pelleted by centrifugation at 350 × g for 7 min at 4° C and resuspended in PBS.

Murine neutrophil isolation

Neutrophils were isolated from murine bone marrow. Long bones were flushed with PBS containing 2 % fetal bovine serum (FBS), to generate a bone marrow (BM) cell suspension. Cells were filtered by using a 40 µm strainer and pelleted at 350 x g for 7 min at 4° C. Erythrocytes were removed by addition of erylysis buffer (155 mM NH_4Cl_2, 10mM $KHCO_3$,

0.1mM EDTA, pH 7.3). Lysis was stopped after 10 min by addition of PBS containing 2 mM EDTA. Cell suspension was washed and neutrophils were isolated using MACS neutrophil isolation kit (Miltenyi Biotec, Germany). Briefly, cells were incubated with MACS negative selection antibody panel before flowing through a LD Column (MACS Miltenyi Biotec, Germany). Isolated neutrophils were pelleted by centrifugation at 350 × g for 7 min at 4° C and resuspended in PBS.

Protein digestion and in-StageTip purification for proteome analysis

Proteomics sample preparation was carried out with the 96-well PreOmics iST kit (P.O.00027) following the manufacturer's protocol. Purified peptide concentration was set to 0.2 mg/ml after determination of concentration by nanodrop. Bear plasma samples were fractionated in three fractions with the PreOmics iST fractionation add-on kit (P.O.00102) according to the manufacturer's protocol.

Phospho-peptide enrichment

27 ng of purified peptides were dried in a 96-well plate (Eppendorf Twintec) and resuspended in enrichment equilibration buffer (1 % (v/v) TFA, 80 % (v/v) acetonitrile). Subsequent to the priming (0.1 % (v/v) TFA in 99 % acetonitrile) of Fe-NTA cartridges, phosphorylated peptides were enriched on the AssayMAP Bravo platform (Agilent Technologies) and eluted from the cartridges (1 % ammonium hydroxide (v/v) in H_2O). All steps were conducted according to the manufacturer's protocol. Resulting peptides were vacuum-dried and resuspended in buffer A* (0.1 % formic acid, 2 % ACN) for LC-MS analysis.

Ultra-high-pressure liquid chromatography and mass spectrometry

Samples were measured using LC-MS instrumentation consisting of an EASY-nLC 1200 ultra-high-pressure system (Thermo Fisher Scientific), which was coupled to an Orbitrap Exploris 480 instrument (Thermo Fisher Scientific) using a nano-electrospray ion source (Thermo Fisher Scientific). Purified peptides were separated on in-house packed columns with a pulled emitter tip (50 cm, 0.75 µm ID, Dr. Maisch Reprosil AQ C-18 beads) (*50*). 200 ng peptides for full proteome analysis and the complete volume of resuspended peptides from enrichment for phospho-peptide analysis were loaded on the column in buffer A*. Column temperature was kept at 60° C by an in-house-developed oven containing a Peltier element.

Bear platelet peptides were eluted with a linear 105 min gradient of 5-30 % of buffer B (0.1 % formic acid, 80 % (v/v) acetonitrile), followed by a 10 min increase to 95 % of buffer B, followed by a 5 min wash of 95 % buffer B at a flowrate of 300 nl/min. MS data was acquired with a Top15 data-dependent MS/MS scan method. MS1 AGC Target was set to 300 % in the 300-1650 m/z range with a maximum injection time of 25 ms and a resolution of 60,000 at m/z 200. Fragmentation of precursor ions was performed by higher-energy C-trap dissociation (HCD) with a normalized collision energy of 30 %. MS/MS scans were performed at a resolution of 15,000 at m/z 200 with an AGC Target of 100 % and a maximum injection time of 28 ms. Dynamic exclusion was set to 30 s to avoid repeated sequencing of identical peptides.

Bear plasma and platelet secretome peptides were eluted with a linear 38 min gradient of 3-30 % of buffer B, followed by a 4.5 min increase to 98 % of buffer B, followed by a 2.5 min wash of 95 % buffer B at a flowrate of 450 nl/min. MS data were acquired with a Top15 data-dependent MS/MS scan method. MS1 AGC Target was set to 300 % in the 300-1650 m/z range with a maximum injection time of 25 ms and a resolution of 60,000 at m/z 200. Fragmentation

of precursor ions was performed by higher-energy C-trap dissociation (HCD) with a normalized collision energy of 27 %. MS/MS scans were performed at a resolution of 15,000 at m/z 200 with an AGC Target of 100 % and a maximum injection time of 25 ms. Dynamic exclusion was set to 30 s to avoid repeated sequencing of identical peptides.

For human phospho-proteome analysis, peptides were loaded and eluted on a 60-min gradient of 3-41 % buffer B, enhanced by a final increase of buffer B to 90 % within 5 min and a wash of 90 % buffer B for 5 min. Data were acquired in DIA mode employing full MS scans (scan range: 300 to 1,400 m/z; resolution: 120,000; maximum injection time: 60 ms) and 32 periodical MS/MS segments applying isolation windows (resolution: 30,000; maximum injection time: 54 ms; normalized AGC target: 1000 %). Peptide fragmentation was enabled by HCD (NCE: stepped, HCD Collision Energies: 25–27.5–30 %).

For platelet proteome analysis of human bed-rest patients, peptides were loaded and eluted on the same gradient as the bear platelet peptides. Data were acquired in DDA mode using full MS scans (scan range: 300 to 1,650 m/z; resolution: 120,000; maximum injection time: 25 ms; normalized AGC target: 300 %) and 62 periodical MS/MS segments applying isolation windows (resolution: 15,000; maximum injection time: 25 ms; normalized AGC target: 300 %). Peptide fragmentation was enabled by HCD (NCE: stepped, HCD Collision Energies: 25–27.5–30 %).

Mass spectrometry data analysis of bear samples

MS raw files were analyzed by MaxQuant software, version 1.6.11.0 (*51*), and peptide lists were searched against the Uniprot fasta database for the organism investigated (Ursus arctos). A contaminant database generated by the Andromeda search engine (*51*) was configured with cysteine carbamidomethylation as a fixed modification and N-terminal acetylation and methionine oxidation as variable modifications. We set the false discovery rate (FDR) to 0.01 for protein and peptide levels with a minimum length of 7 amino acids for peptides, and the FDR was determined by searching a reverse database. Enzyme specificity was set as C-terminal to arginine and lysine as expected using trypsin and LysC as proteases. A maximum of two missed cleavages were allowed. Peptide identification was performed with an initial precursor mass deviation up to 7 ppm and a fragment mass deviation of 20 ppm. All proteins and peptides matching to the reversed database were filtered out.

Mass spectrometry data analysis of human phosphoproteome

MS raw files of the human phosphorylation data concerning treatment with SMI I were analyzed by Spectronaut software version 15.1.210713 (Biognosys, Switzerland) in reference to the human Uniprot FASTA database (standard and additional). Enzymatic cleavage was defined by Trypsin/P, and phosphorylation at serine, threonine, or tyrosine was added as variable modification to default settings. We included peptide lengths of 7-52 amino acids and limited the maximum number of missed cleavages to 2. The FDR threshold for peptides was set to 0.01 while PTM localization filtering was disabled. MS raw files of the human phosphorylation data concerning treatment with SMI II were analyzed with DIA-NN software version 1.8.1 (*49*) Setting details have been deposited to the ProteomeXchange Consortium via the PRIDE partner repository and are available via ProteomeXchange with identifier PXD039087.

Mass spectrometry data analysis of human bed-rest patient platelets

MS raw files of the human platelet proteome data were analyzed by Spectronaut software version 15.6.211220.50606 (Biognosys, Switzerland) in reference to the human Uniprot fasta database (standard and additional). Enzymatic cleavage was defined by Trypsin/P. We included peptide lengths of 7-52 amino acids and limited the maximum number of missed cleavages to 2. The FDR threshold for peptides was set to 0.01 while PTM localization filtering was disabled.

Homology matching of human to bear protein sequences

Homology matching of bear (Ursus arctos) and human protein sequences was done using a local installation of the Blast+ Command Line Applications (v2.12.0). Fasta files were obtained from Uniprot. Human fasta files were combined and converted into a Blast database using the makeblastdb tool. Mapping of the bear sequences was done using the blastp command, applying standard settings and using the previously generated human database. The resulting output file was filtered, retaining for each bear protein the match with lowest E-value and highest sequence identity. In case more than one sequence fulfilled these criteria, all were kept in the final output.

Light transmission aggregometry

Light transmission aggregometry (Optical aggregometer, Model 700, Chrono-Log Corporation, US) was performed in washed platelets (final concentration 100.000 PLTs/µl) in a total volume of 300 µl Tyrode's Buffer (pH 7.4) in the presence of 1 mM Mg^{2+} and Ca^{2+}. Aggregation was triggered by the following agonists. Bears: 10 µg/ml or 20 µg/ml collagen, 20 µM ADP, 16 mM thrombin receptor activating peptide (TRAP), 2 µM U46619, 0.01 U/ml or 0.1 U/ml thrombin; human: 5 µg/ml fibrillar collagen (ChronoLog Corporation, US) and 0.1 U/ml thrombin. If indicated, samples were pre-incubated with HSP47 inhibitor (50 nM; Col003, MedChemExpress, US) for 15 min. Aggregation responses were quantified as maximum aggregation.

Platelet spreading analysis (bears and humans)

Coverslips were coated with 100 µg/ml fibrinogen (Sigma-Aldrich, Germany), 50 µg/ml fibronectin (Sigma-Aldrich, Germany) or 50 µg/ml rat tail collagen I (Sigma-Aldrich, Germany) for 1 h at 37° C and washed afterwards with PBS. Washed platelets were stimulated with 0.1 U/mL thrombin or 10 µg/ml fibrillar collagen (ChronoLog Corporation, US) and seeded on cover slides. After 8, 15 and 30 min platelets were fixed with 4 % paraformaldehyde (PFA), permeabilized with 0.5 % Triton X-100 and stained with phalloidin 488 (1:1000; ThermoFischer, US). If indicated, platelets were incubated with HSP47 antibody (1:1000; clone: M16.10A1; Enzo Life Science, US). Images were acquired using a ZEISS LSM 800 confocal microscope and analyzed by ZEN blue, ZEN black software (ZEISS, Germany) or Image J software.

Thromboelastographic analysis

Thromboelastographic analysis was performed using ROTEM® system (TEM Innovations, Germany) for bears and ClotPro® system (Enicor, Germany) for human samples. Both systems are clinically calibrated and approved. Briefly, citrate whole blood from bears or

humans was stimulated with EXTEM, INTEM or FIBTEM stimulus at 37° C or 33° C for winter bear samples.

Determination of circulating DNA and citrullinated histone H3

Circulating DNA and citrullinated histone H3 (citH3) was quantified in citrate plasma using commercially available ELISA kits (circulating DNA quantification kit, Abcam, Germany; citrullinated histone H3, Cayman, US) and performed according to the manufacturer's protocol. Briefly, DNA was isolated from citrated plasma, stained and analyzed by fluorescence reader (TECAN, Switzerland). CitH3 was quantified from plasma samples by sandwich ELISA.

Determination of citrullinated histone H3 DNA complexes

CitH3-DNA levels in plasma from hibernating and active brown bears (supernatant from bear neutrophils stimulated with PMA was used as positive control) were quantitively analyzed *(52)*. Briefly, plasma samples diluted 1:5 with detection antibody anti-DNA POD (Cell Death Detection ELISA PLUS Kit, Roche, Switzerland) were used for this purpose. 96-well microplates were incubated with abR8Cit-1c at a concentration of 5 µg/mL overnight and then washed with Tween/PBS (0.05 %) and blocked with BSA/PBS (5 %) for 1.5 h. As a standard, a dilution H3R2,8,17Cit dNucs (EpiCypher #16-1362) was prepared in descending 2-fold dilution and finally standard was prepared at the concentrations of 1000, 500, 250, 125, 62.5, 31.3, 15.6, and 0 ng/mL in standard diluent (50 mmol/L Tris-HCl pH 7.5, 0.01 % BSA/PBS). Then, the plasma samples were loaded into the well plates and incubated for 2 h on a 300 rpm horizontal shaker. Subsequently, the plates were washed 3 times with Tween/PBS (0.05%) and horseradish peroxidase (HRP) substrate (Thermo Fisher Scientific, USA) was added. After the samples turned to a dark blue, the optical density was determined (Tecan, Switzerland). The concentration of citH3-DNA plasma level was determined and calculated based on the relations to the standard curve.

Platelet specific flow cytometry

To perform flow cytometry and t-Distributed Stochastic Neighbor Embedding (t-SNE), platelets were multi-color labelled using the following antibodies: CD41 (PE/Cy5, clone: HIP-8, BioLegend, Germany), CD41/CD61 (AF647, Clone PAC-1, BioLegend, Germany), CD62P (AF700, Clone AK-4, BioLegend. Germany), CD29 (PE, Clone Mar04, BD Biosciences, US), GPVI (BV421, Clone HY101, BD Biosciences, US), CD61 (PE/Dazzle 594, Clone VI-PL2, BioLegend, Germany), CD42b (BV650, Clone HIP-1 BioLegend,Germany), CD154 (BV510, Clone 24-31, BioLegend, Germany) CD63 (APC/Cy5, Clone H5C6, BioLegend, Germany) and HSP47 (FITC, Clone G-12, Santa Cruz Biotechnology, US). Cells were stimulated with the either thrombin (0.1 U/ml) or collagen (10 µg/ml) in the presence or absence of HSP47 inhibitor (50 nM). Data were analyzed by FlowJo (v. 10.6.1, US) and if indicated t-SNE and FlowSOM plugins were used. After down sampling with the Downsample V3 plugin and concatenation step, t-SNE (t-SNE Plugin, FlowJo v. 10.6.1, US) was performed on equal cell numbers for both treatment groups. The individual subpopulations were identified and subclustered using FlowSOM (FlowSOM Plugin for FlowJo v. 10.6.1, US). Relative mean MFI values are given in arbitrary units, heat map was generated by FlowSom. For SCI and acutely immobile patients, washed platelets were labelled with the following antibodies: CD62P (PE, Clone Mar04, BD Biosciences, US), active GPIIbIIIA (AF647, Clone PAC-1, BioLegend, Germany), CD 63 (APC/Cy5, Clone H5C6, BioLegend, Germany), GPVI (BV421, Clone HY101, BD Biosciences, US), GP2bα (PE/Cy5, clone: HIP-8, BioLegend, Germany), HSP47 (FITC, Clone G-12, Santa Cruz Biotechnology, US). In immobile pigs, HSP47 expression was analyzed in

washed platelets after labelling with HSP47 (FITC, Clone G-12, Santa Cruz Biotechnology, US).

Thrombin-Binding-Assay

Thrombin binding to human and murine platelets was determined by flow cytometry. Platelets were isolated as described above. Human platelets were incubated with either HSP47 small molecule inhibitor (SMI) I (50 nM; Col003, MedChemExpress, US), SMI II (66 µM; RH00007SC; Maybridge, Thermo fisher scientific, UK), or the vehicle (DMSO) for 15 min at 37° C. Thereafter, platelet reactivity was inhibited by the addition of 7500 units of lepirudin. Binding of fluorescence labelled thrombin was determined by flow cytometry after stimulation with 1 U/ml thrombin for 15 min. In SCI patients and healthy controls as well as HSP47 knock-out mice thrombin-binding was measured at baseline conditions.

Prostacyclin ELISA

Prostacyclin levels in bear plasma were determined using a conventionally available ELISA kit (Prostacyclin ELISA Kit OKEH02555, AVIVA Systems Biology, San Diego, California, USA) and performed according to the protocol provided by the company.

Echocardiographic analysis of right ventricular function in hibernating bears

For analysis of right ventricular diameter, earlier acquired echocardiographic images underwent re-analysis for this study *(9)*. Echocardiography was performed in the field with the bear in a left lateral recumbency using a Phillips CX50 with an S51 probe, and right ventricular diameter was measured in the apical four-chamber view (cm).

Neutrophil Activation Assays

Reactive Oxygen Species (ROS)-levels and CD11b expression were determined in human neutrophils isolated from EDTA-anticoagulated whole blood using a BD LRS Fortessa Flow Cytometer. Neutrophils were stimulated as indicted with HSP47 peptide (10 ng/ml or 100 ng/ml), LPS (Lipopolysaccharide, 20 µg/ml), Pam3CSK4 (Pam3CysSerLys4, 5 µg/ml) or fMLP (N-Formylmethionine-leucyl-phenylalanine; 10 µM) for 1 h at RT after inhibition with TLR-2 inhibitor (150 µM; TL2-C29, invivogen, San Diego, California, US)), TLR-4 inhibitor (30 µM; NBP2-26244; Novus Biologicals, Colorado, USA) or MYD88 inhibitor (1 µM; Pepinh-MYD-88 inhibitor; MyD88 inhibitor peptide invivogen, San Diego, California, USA) if indicated. Cells were subsequently stained for CD16 (APC, Clone 3G8, BioLegend, Germany) to identify neutrophils or with 10 nM 2′,7′-Dichlorodihydrofluorescein diacetate (DCFDA) for 30 min to determine intracellular ROS level or CD11b (BV605, Clone ICRF44, BioLegend, Germany) expression. MFI ratio were determined using FlowJo software (FlowJo v. 10.6.1). Neutrophil NET formation upon HSP47 stimulation was quantified by confocal microscopy. Briefly, neutrophils were stimulated with HSP47 peptide (10 ng/ml or 100 ng/ml), fMLP (10 µM) or co-stimulated with fMLP (10 µM) + HSP47 peptide (10 ng/ml or 100 ng/ml) and seeded on poly-L-lysine (602895, Sigma Aldrich, Germany) coated coverslips. After 1 h at 37° C cells were fixed with 4 % PFA, permeabilized (0.5 % Triton X-100) and stained with SytoxGreen (500 nM, Thermo Fisher Scientific, US) and Hoechst dye (1:1000, Invitrogen, US). Cells were visualized by immunofluorescence microscopy (4 fields of 20 times enlarged). NETs were defined as SytoxGreen positive extracellular structures. NET forming neutrophils are shown as percentage of all neutrophils.

NET formation in platelet-neutrophil co-culture

Thrombin (0.1 U/ml) or collagen (5 µg/ml) pre-activated platelets were seeded on poly-L-lysine (602895, Sigma Aldrich) coated coverslips. After 15 min neutrophils were added and incubated for 1 h at 37° C. Then, cells were fixed with 4 % PFA, permeabilized (0.5 % Triton X-100) and stained with anti-myeloperoxidase (MPO, R&D Systems, US), anti-citrullinated histone H3 (Abcam, Germany), and Hoechst dye (Hoechst 33342, Invitrogen, US). Cells were visualized by immunofluorescence microscopy (4 fields of 20 times enlarged). NETs were defined as extracellular structures with a size over 5 µm, connected to MPO-positive cells and stained positive for MPO, citH3 and Hoechst. NET forming neutrophils are shown as percentage of all neutrophils. Neutrophil platelet aggregates were determined after platelet activation with thrombin (0.1 U/ml) following incubation with SMI I (50 µM; Col003; MedChemExpress, US) or SMI II (66 µM; RH00007SC; Maybridge, Thermo fisher scientific, UK) if indicated at RT for 30 min using flow cytometry. Samples were labelled with CD41 (PE/Cy5, clone: HIP-8, BioLegend, Germany), CD 16 (FITC, Clone 3G8, BioLegend, Germany) and then evaluated using FlowJo Software (FlowJo v. 10.6.1, BD Biosciences, US).

NET formation assay in humans and bears

Neutrophil granulocytes were isolated according to previously described protocols. Neutrophils were stimulated with HSP47 peptide (10 ng/ml or 100 ng/ml), fMLP (10 µM), PMA (Phorbol-12-myristat-13-acetat; 50 nM) or co-stimulated with fMLP (10 µM) + HSP47 peptide (10 ng/ml or 100 ng/ml) and seeded on poly-L-lysine (602895, Sigma Aldrich) coated coverslips. After 1 h at 37° C cells were fixed with 4 % PFA, permeabilized (0.5 % Triton X-100) and stained with SytoxGreen (Thermo Fisher Scientific, US, S7020, 500 nM final concentration) and Hoechst dye (Hoechst 33342, Invitrogen). Cells were visualized by immunofluorescence microscopy (4 fields of 20 times enlarged). NETs were defined as SytoxGreen positive extracellular structures. NET forming neutrophils are shown as percentage of all neutrophils.

Coagulation factor analysis

Activity of coagulation factors VIII, IX, XI and XII was analyzed using one-stage assay with human factor deficient plasma. Due to limited amount of available plasma samples, not all coagulation factors could be tested.

Immunoblotting for HSP47

Platelets from brown bears, HSP47 knock-out mice, patients with SCI, or individuals on bed rest (isolated as described above) as well as neutrophil granulocytes, monocytes, B cells, and T cells (isolated with MACS Miltenyi Biotec isolation kits according to the manufacturer's protocol) were lysed and subjected to immunoblotting. The blotting membrane (PVDF) was incubated with an antibody against HSP47 (1:1000; clone:M16.10A1, Enzo Life Science, US) and subsequently probed with HRP-coupled secondary antibody (Goat anti-mouse IgG-HRP conjugated, Bio-Rad Laboratories, US). Chemiluminescence signals were detected by Western blot imaging system (Amersham ImageQuant 800, Cytiva, US) after addition of chemiluminescent detection reagent to the membrane (ECL, Merck, Germany). To show equal loading, membranes were reprobed with an antibody against β-actin (1:1000, 13E5 Rabbit mAb HRP conjugated, Cell Signaling, US) or GAPDH (1:1000, thermofisher).

Quantitative real-Time PCR for platelet gene expression

Patient platelet mRNA was isolated with TRIzol and reverse transcribed to cDNA template with High Capacity cDNA Reverse Transcription kit (Thermo Fischer) according to the manufacturer's protocol. All q-PCR experiments were performed using SYBR GREEN and detected with BIO-RAD MyiQ real-time detection system. For each tested gene, expression of beta-actin was used as the internal control and the mean threshold cycle number (mean Ct value) of each tested gene was used to quantify the relative gene expression in platelets. All primers (HSP47, Itga2b, GP6 and beta-actin) used in real-time PCR were purchased from Qiagen company (Cat#QT00044709, Cat#QT00037345, Cat#QT01003121, Cat#QT00095431).

Histological analysis

Vena cava thrombi were embedded in Tissue-TEK (Sakura, US) and frozen at -80° C. Tissue samples were cut with a cryotome (CryoStar NX70, ThermoFisher Scientific, US) into 10 µm sections, fixed with 4 % formaldehyde and blocked with 5 % BSA in PBS. Sections were incubated with primary antibodies for citH3 (488, Clone: ab5103, Abcam, US) and MPO (647, clone A039829, DAKO, US). DNA was stained with 1 µg/mL Hoechst dye (Hoechst 33342, Invitrogen, Germany). Pictures were acquired using a ZEISS LSM 800 confocal microscope (Zeiss, Germany) and analyzed using Imaris software (Imaris v. 8.0.1, Bitplane, UK). For identification of NETs, two distinct criteria had to be met: (1) NET structures are triple positive for citH3, MPO and DAPI and (2) NETs originate from MPO positive cells.

Bed rest study

After providing written informed consent, 4 Caucasian women and 8 Caucasian men aged between 25 and 51 years (35 ± 10 years, weight: 77 ± 11 kg, height: 176 ± 8 cm, BMI: 25 ± 3 kg/m^2), participated in the Spaceflight-Associated Neuro-ocular Syndrome Countermeasure Study (SANS). SANS was a joint project between the National Aeronautics and Space Administration (NASA) and the German Aerospace Center (DLR). All participants had no history of cardiovascular disease or thromboembolic incidences, took no medication, and were non-smokers for at least 6 months prior to enrolment. Prior to study inclusion all participants successfully passed a thrombophilia screening which excluded candidates with pathological values of international norm ratio, partial thromboplastin time, thrombin clotting time, concentrations of factors I and VIII, lupus anticoagulant and activities of protein s and protein c. Furthermore, factor II (prothrombin) and factor V Leiden mutations were excluded by genetic analysis. The study was conducted in accordance with the declaration of Helsinki. The protocol was approved by the ethics commissions of the Medical Association North Rhine (number 2020211) and NASA (Johnson Space Center, Houston, United States).

The overreaching goal of SANS was to assess adaptations of the eye and the brain evoked by 30 days of strict head down tilt bed rest. Strict bed rest, the gold standard of chronic weightlessness simulation on earth for human studies (*53*), means that all daily activities including personal hygiene were done in a clinical bed in the −6° Trendelenburg position. Including the pre and post bed rest phases, the participants spent 58 days at the DLR Envihab research facility in Cologne, Germany. All participants ingested standardized isocaloric diets with controlled fluid intake and were subjected to regulated bed times. Caffeine or alcohol containing beverages were not allowed. Participants did not receive prophylactic anticoagulants during bed rest, however, ibuprofen was allowed as pain reliever. Participants did not exercise at least 24 h before we performed our blood draws. After a 14-day ambulatory phase for

familiarization to the test facility, participants spent 30 days in strict bedrest. The bed rest period was followed by 14 days of re-ambulation (recovery). Blood was drawn through an intravenous line placed in an antecubital vein into a heparinized syringe followed by immediate buffering and slow freezing at -80° C. Blood draws were performed within two days before start of bedrest and after 27 days of strict bed rest. Flow cytometry analysis was performed on 10 individuals.

Statistical analyses

Statistical analysis was conducted using GraphPad Prism® software (GraphPad Software Inc). Shapiro-Wilk test, D'Agostino-Pearson omnibus test were used to test for normality distribution. Normally distributed data were tested using unpaired t-test, non-normally distributed data using the Mann-Whitney U-test. Repeated measurements were analyzed using paired t-test or Wilcoxon matched pairs test. To enhance statistical power, we performed serial measurements on samples from the same brown bears, acutely immobile patients, and bed resting individual as paired data sets. In vitro assays performed with samples from the same individual under different conditions were also analyzed as paired samples. Whenever different mice or patients with SCI were studied, we performed an unpaired analysis. For multiple groups testing, ANOVA analysis was conducted after testing for homogeneity of variance using the Brown-Forsythe test. Data are means ± standard deviation (SD) and mean difference with 95 % confidence intervals (CI).

Bioinformatics analysis of proteomics data

Proteomics data were analyzed with Perseus software package (version 1.6.2.3) including the Perseus plugin peptide collapse *(46)* and in Python (version 3.6.4.) using NumPy (1.19.2), Pandas (1.1.4) and Matplotlib (3.3.2) packages *(54,55)*. The MS-based proteomics data have been deposited to the ProteomeXchange Consortium via the PRIDE partner repository and are available via ProteomeXchange with identifier PXD030465, PXD031521 and PXD039087.

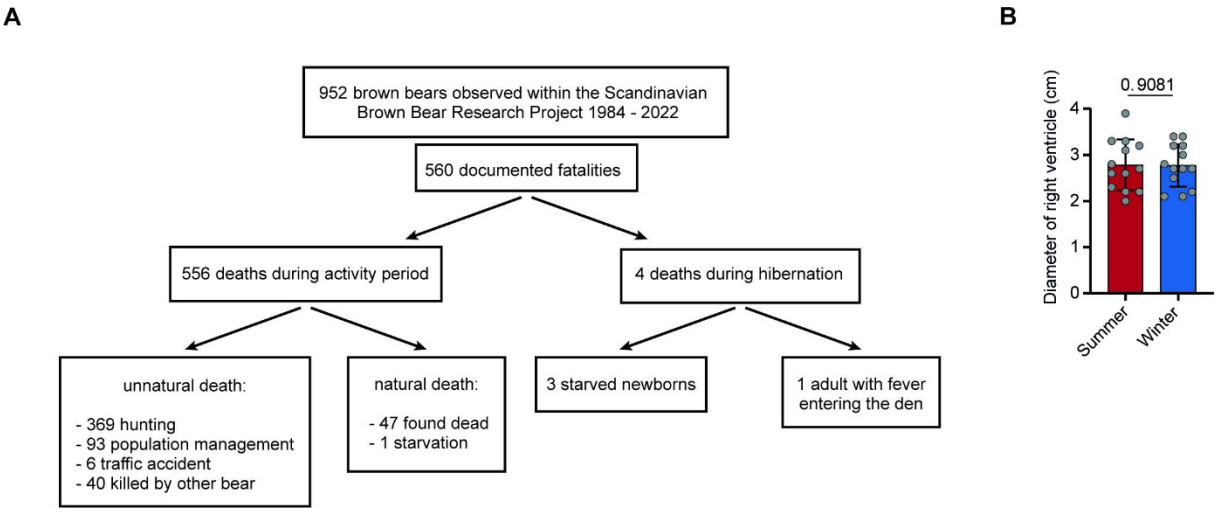

Fig. S1. Venous thromboembolism in brown bears

(A) Fatalities of brown bears observed within the Scandinavian Brown Bear Research Project between 1984 and 2022. (B) Echocardiographic analysis of right ventricle diameter of hibernating and active brown bears (n = 13; symbols represent individuals; data show means ± SD). P-values were determined with paired t-test.

A

		Winter (n=13)	Summer (n=13)	p-value
WBC	10^9/l	4.7±0.9	5.9±2.5	0.0923
LYM*	%	29.2±7.4	24.7±9.2	0.0754
MON*	%	8.0±..4	7.9±2.2	0.9284
NEU*	%	43.1±8.2	54.5±14.1	0.0204
EOS*	%	19.8±8.8	13±.4.0	0.1037
HGB	g/dl	20.8±1.3	15.6±1.2	<0.0001
RBC	10^{12}/l	8.4±0.7	6.1±0.3	<0.0001
PLT	10^{3}/l	274.5±94.5	442.2±156.1	0.0019
MPV	fl	5.2±0.5	4.7±0.4	0.0071

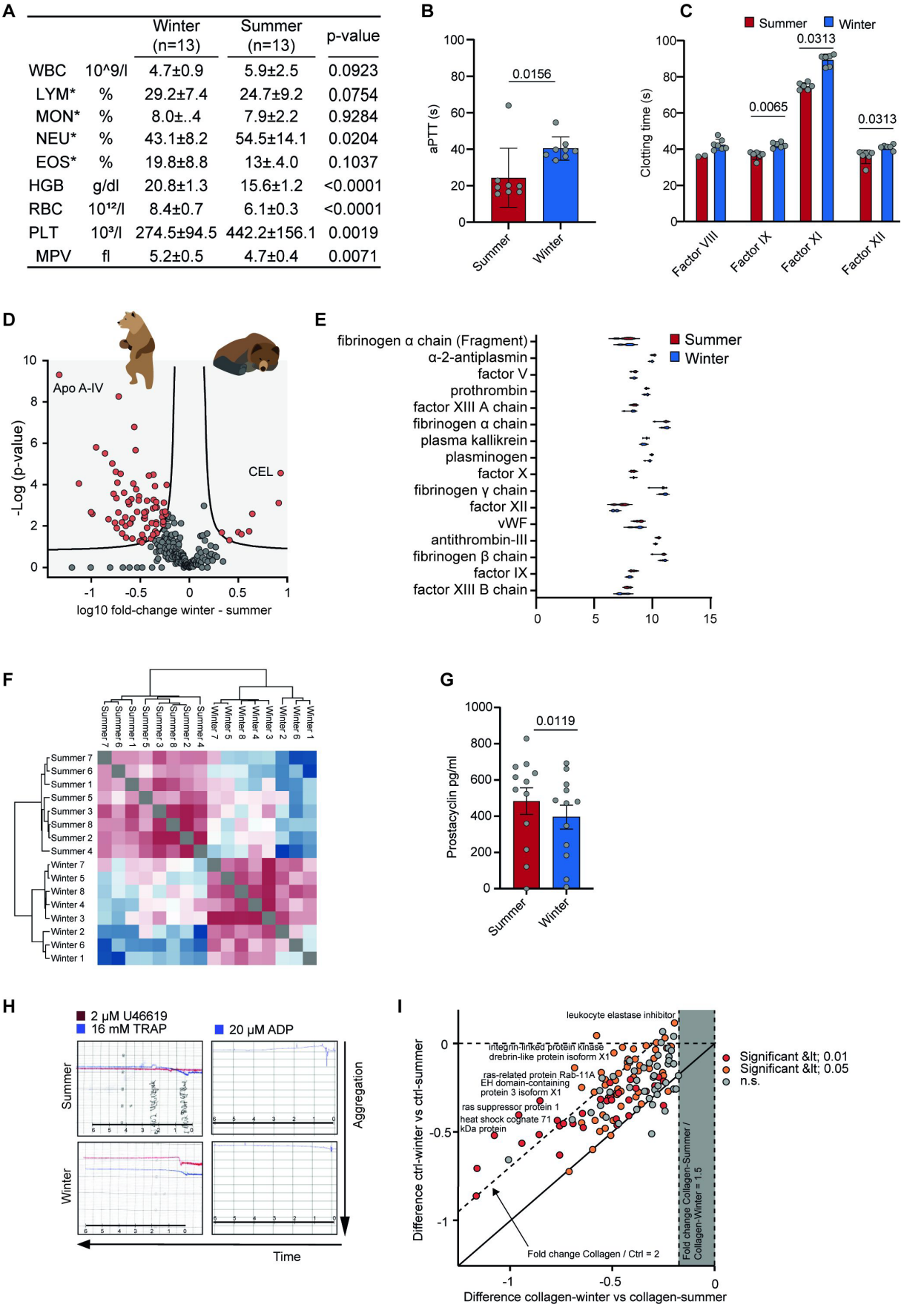

Fig. S2. Seasonal differences in bear blood and plasma

(A) Hematological characterization of hibernating and active bears. Blood count analysis is shown (n = 13; * n = 8; p-values were determined using paired t-test for lymphocytes (LYM), monocytes (MON), neutrophils (NEU), eosinophils (EOS), hemoglobin (HGB), platelets (PLT) and mean platelet volume (MPV); Wilcoxon test was used for white blood cells (WBC) and red blood cells (RBC)). (B) Analysis of activated partial thromboplastin time (aPTT) in citrate plasma in active and hibernating brown bears (n = 8; data shown as means ± SD; p-values were determined using Wilcoxon test). (C) Detailed analysis of intrinsic coagulation pathway (factor VIII: n = 2 for summer, n = 7 for winter; factor IX: n = 6; factor XI: n = 6 factor XII: n = 6; p-values were determined using paired t-test for factor IX and Wilcoxon test for factors XI and XII). Symbols represent individual bears; data shown as means ± SD. (D) Plasma proteome analysis in hibernating and active bears (unpaired analysis of 8 individuals). (E) Seasonal differences of plasma protein intensities from MS-based proteomics analysis are shown. Violins represent the protein intensity distributions of 8 individuals during hibernation or active phase. (F) Plasma proteome correlation (Pearson) of 8 individuals from summer and winter shows higher seasonal than intra individual correlation of proteome signatures. (G) Prostacyclin concentrations in paired hibernating and active bears (n = 12; symbols represent individual bears; data shown as means ± SD; p-values were determined using paired t-test). (H) Light transmission aggregometry of washed platelets from active (summer) or hibernating (winter) brown bears was performed after stimulation with the indicated agonists. Representative aggregation curves are shown. (I) Zoomed-in view of the secretome analysis from collagen-stimulated bear platelets (winter vs. summer; Figure 2D). Proteins annotated with protein name in the upper left area of the plot are secreted specifically upon collagen stimulation of summer platelets.

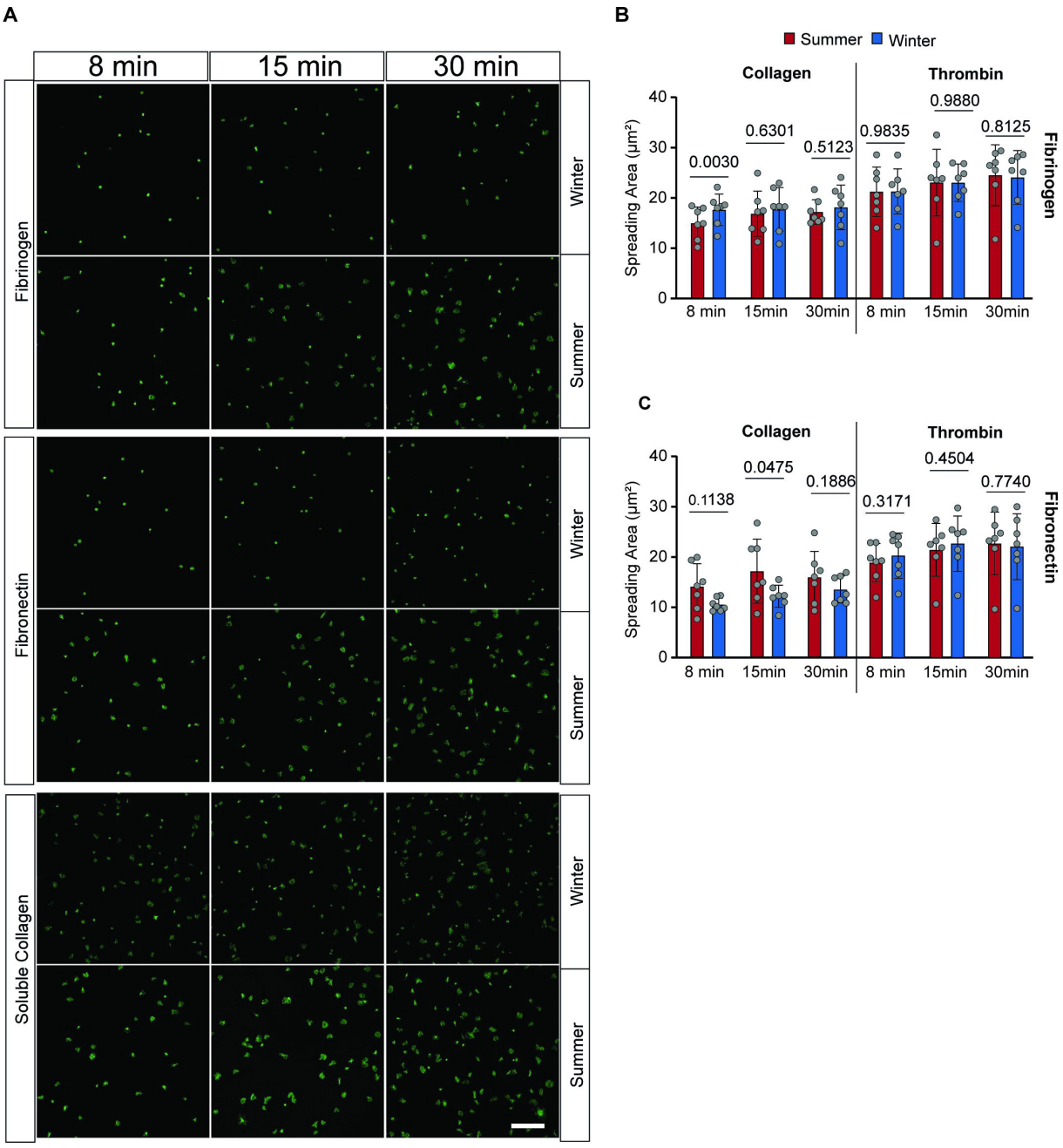

Fig. S3. Seasonal differences in bear platelet population

(A) Representative images of platelet spreading after 8, 15 and 30 minutes following collagen simulation; scale bar represents 20 µm. (B-C) Spreading size of individual platelets stimulated with 10 µg/ml fibrillar collagen or 0.1 U/ml thrombin on fibrinogen (B) and fibronectin (C) coated surfaces was analyzed after 8, 15 and 30 minutes (n = 7; symbols represent individual bears; data shown as means ± SD; all p-values were determined using paired t-test, except of spreading on fibrinogen and stimulation with thrombin after 30 min which was analysed using Wilcoxon test).

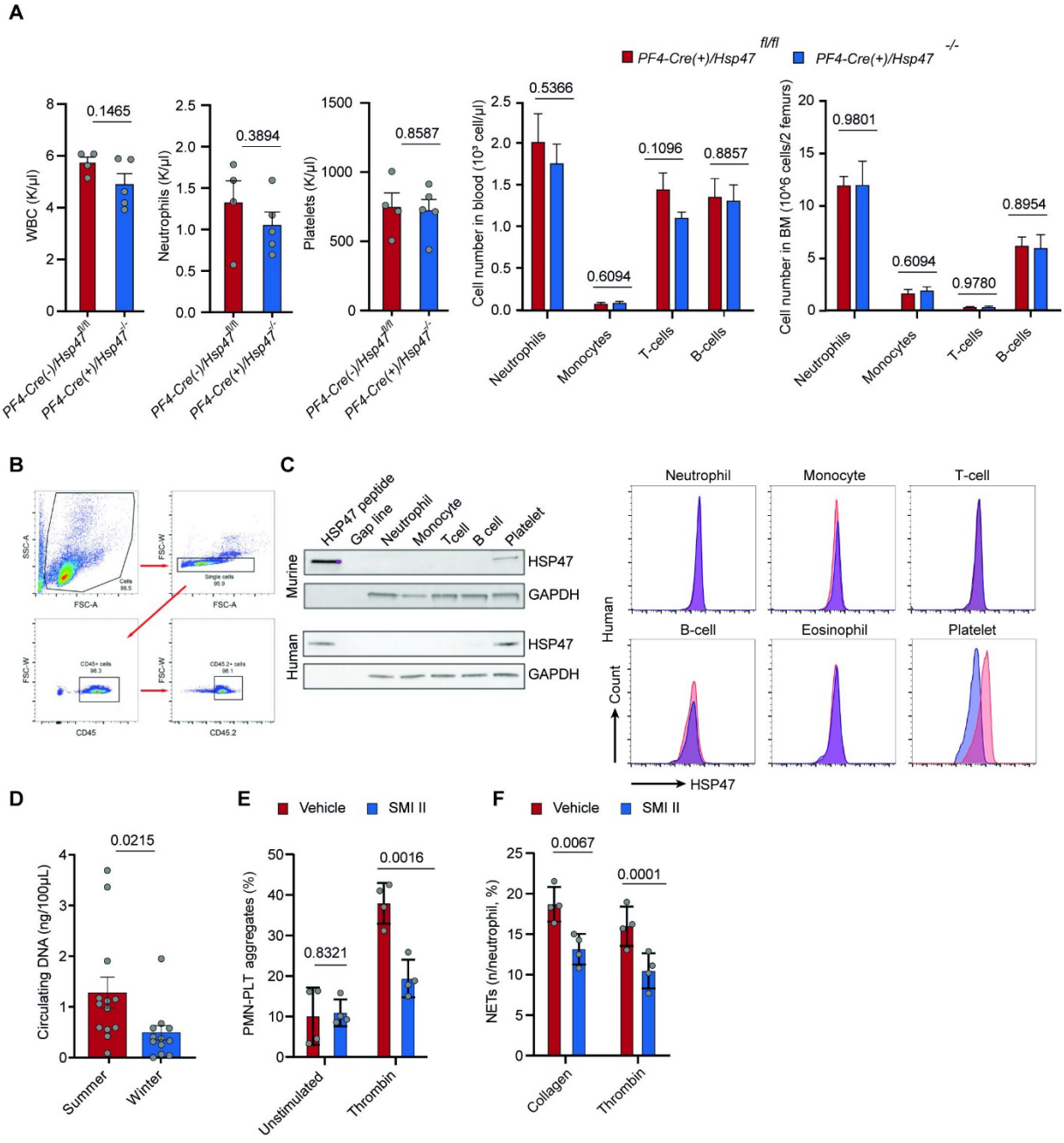

Fig. S4. Characterization of *PF4-Cre/HSP47$^{fl/fl}$* mice

(A) Analysis of peripheral blood counts and bone marrow leukocyte populations (by flow cytometry) of bone marrow chimeras, reconstituted with *PF4-Cre(-)/HSP47$^{fl/fl}$* or *PF4-Cre(+)/HSP47$^{-/-}$* bone marrows (n = 5) and littermate controls (n = 4; data shown as means ± SD; p-values were determined using unpaired t-test for white blood cells, neutrophils and platelets; multiple t-test was used for cells in blood and bone marrow). (B) Determination of peripheral chimerism by flow cytometry in chimeric *PF4-(Cre)/HSP47* mice. Gating strategy to quantify CD45+ positive leukocytes is shown. (C) Representative immunoblots of three independent experiments for HSP47 in murine and human neutrophils, monocytes, T-cells, B-cells and platelets are shown. HSP47 expression by flow cytometry on human neutrophils, monocytes, T-cells, B-cells, eosinophils and platelets. Representative flow cytometry histogram is shown. (D) Circulating DNA levels in hibernating and active bears (n = 12, symbols represent individual bears; data shown as means ± SD; p-values were determined using Wilcoxon test) (E) Quantification of platelet-PMN aggregates following platelet stimulation with thrombin in presence or absence of SMI II (RH00007SC; n = 4; symbols represent individuals; data shown

as means ± SD; p-values were determined using paired t-test). (F) Quantification of NETs per neutrophil after stimulation of platelets with the indicated agonist in presence or absence of SMI II (RH00007SC, bars represent means ± SD; symbols represent single controls; n = 4 per group; p-values were determined using paired t-test).

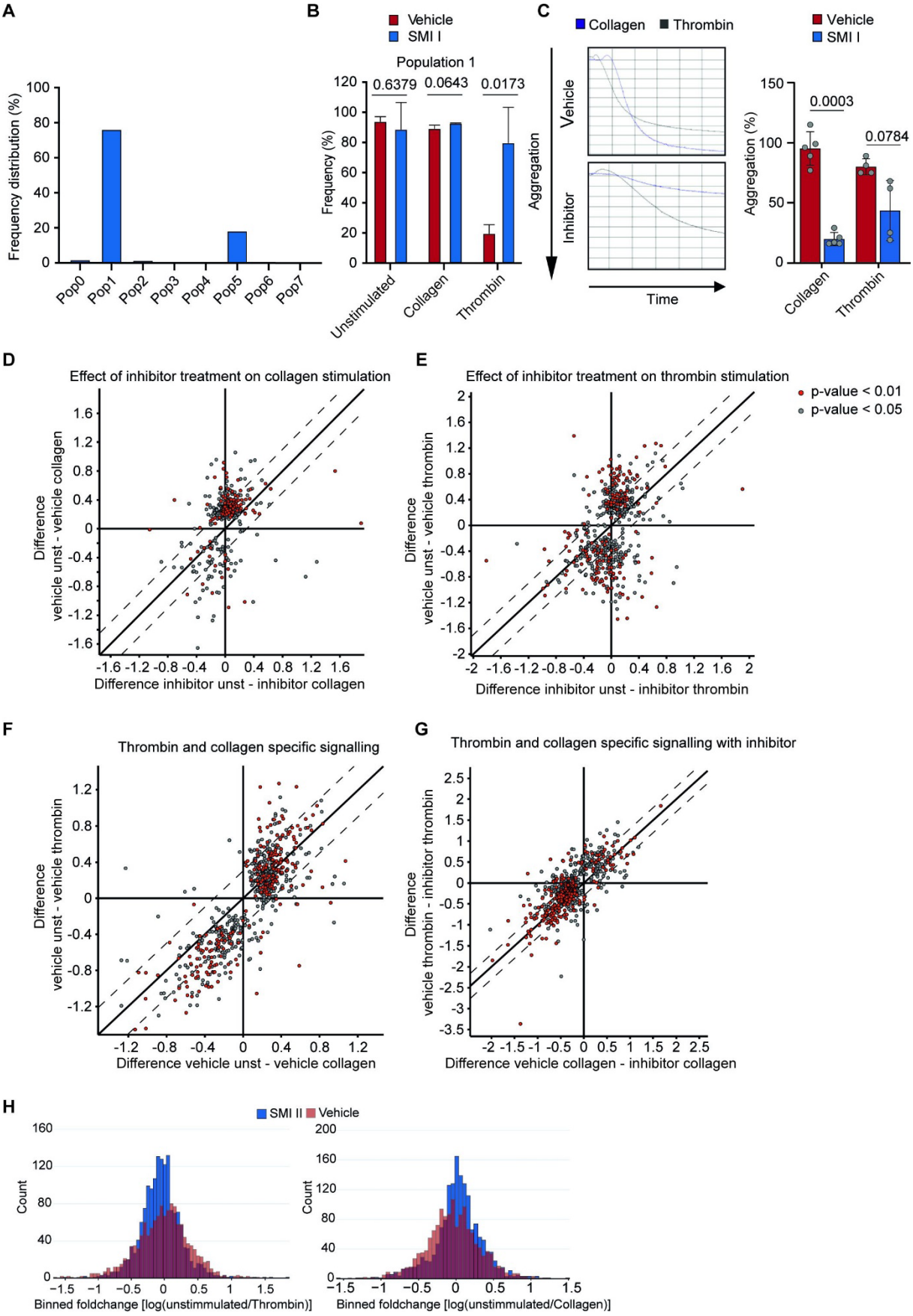
A
Frequency distribution (%)
Pop0
Pop1
Pop2
Pop3
Pop4
Pop5
Pop6
Pop7
B
Vehicle
SMI I
Population 1
Frequency (%)
0.6379
0.0643
0.0173
Unstimulated
Collagen
Thrombin
C
Collagen
Thrombin
Vehicle
Inhibitor
Aggregation
Time
Vehicle
SMI I
Aggregation (%)
0.0003
0.0784
Collagen
Thrombin
D
Effect of inhibitor treatment on collagen stimulation
Difference vehicle unst - vehicle collagen
Difference inhibitor unst - inhibitor collagen
E
Effect of inhibitor treatment on thrombin stimulation
p-value < 0.01
p-value < 0.05
Difference vehicle unst - vehicle thrombin
Difference inhibitor unst - inhibitor thrombin
F
Thrombin and collagen specific signalling
Difference vehicle unst - vehicle thrombin
Difference vehicle unst - vehicle collagen
G
Thrombin and collagen specific signalling with inhibitor
Difference vehicle thrombin - inhibitor thrombin
Difference vehicle collagen - inhibitor collagen
H
SMI II
Vehicle
Count
Binned foldchange [log(unstimmulated/Thrombin)]
Binned foldchange [log(unstimmulated/Collagen)]

Fig. S5. Effects of HSP47 inhibition on platelet function

(A) Multi-color flow cytometry of platelet population following activation with indicated stimuli in the presence or absence of SMI I (Col003). Overall frequency of platelet populations is shown (n = 4; bars show means ± SD). (B) Frequency distribution in population 1 upon stimulation following SMI I (Col003) or vehicle treatment is shown (n = 4; bars show means ± SD; p-values were determined using paired t-test). (C) Light transmission aggregometry of washed platelets after SMI I (Col003) or vehicle treatment upon stimulation with collagen (n = 5) or thrombin (n = 4). Maximum aggregation was determined after 6 minutes; bars show means ± SD; p-values were determined using paired t-test. Representative aggregation curves are shown. (D-E) The effect of HSP47 inhibition upon collagen (D) or thrombin (E) stimulation on the platelet phosphoproteome is shown. The reduced global protein phosphorylation upon inhibition described in Fig. 3B is visible at the individual protein level. Only proteins with a t-test p-value < 0.05 are shown. Dashed horizontal lines indicate a 2-fold difference between the axis conditions. Symbols represent individual proteins; p-values are shown by color coding of symbols. (F-G) Thrombin and collagen stimulation specific phosphoproteome changes in platelets without (F) and with (G) SMI I treatment are shown. Only proteins with a t-test p-value < 0.05 are shown. Dashed horizontal lines indicate a 2-fold difference between the axis conditions. Symbols represent individual proteins; p-values are shown by color coding of symbols. (H) Changing peptides from phospho-proteome analysis of activated platelets under SMI II treatment compared to vehicle treatment after collagen/thrombin stimulation. The phosphoproteome of 6 individuals was compared by independent t-test and average fold changes of all peptides are displayed in the histograms.

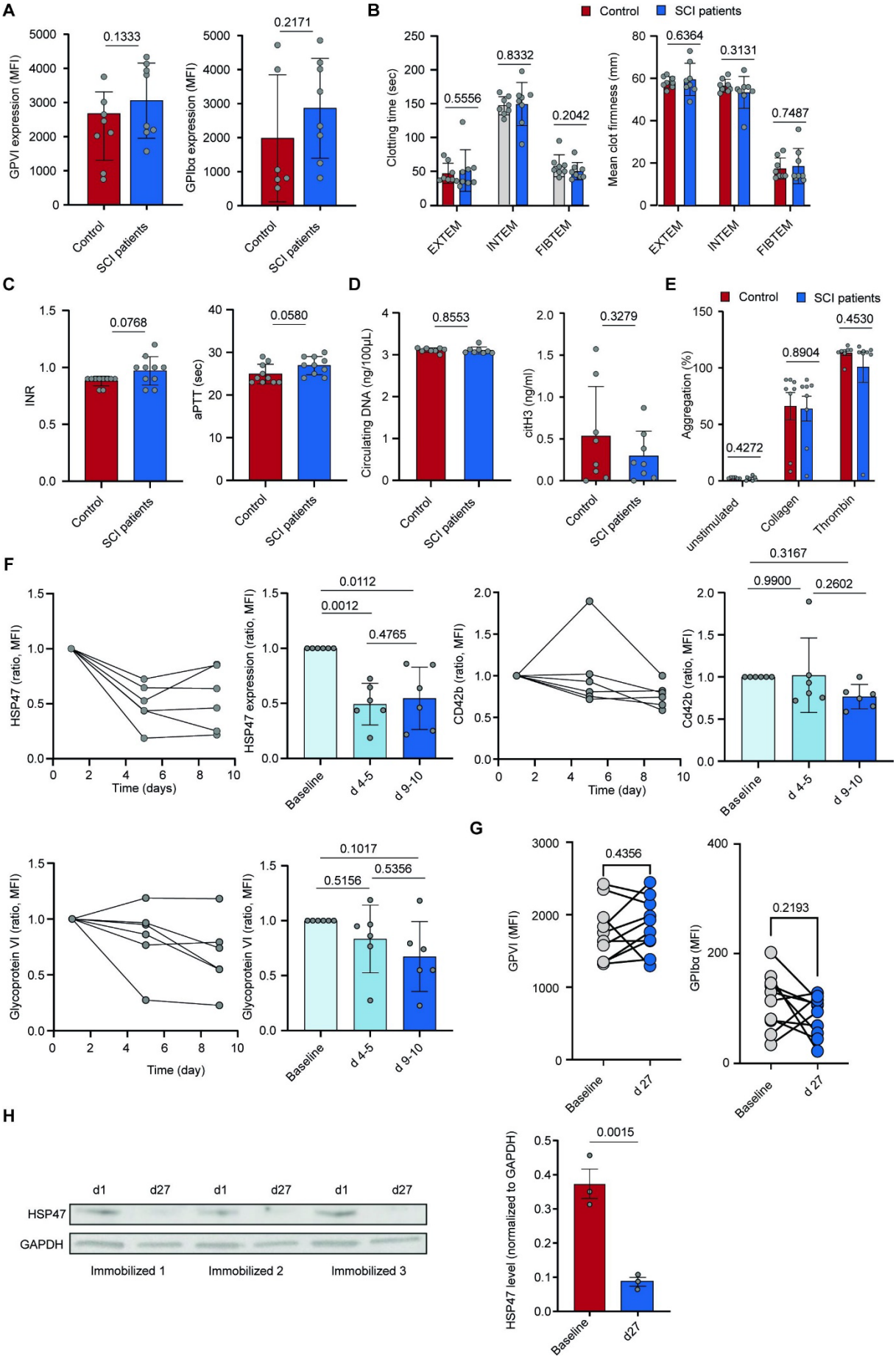
A
GPVI expression (MFI)
0.1333
Control
SCI patients
GPIbα expression (MFI)
0.2171
B
Control
SCI patients
Clotting time (sec)
0.5556
0.8332
0.2042
EXTEM
INTEM
FIBTEM
Mean clot firmness (mm)
0.6364
0.3131
0.7487
C
INR
0.0768
aPTT (sec)
0.0580
D
Circulating DNA (ng/100µL)
0.8553
citH3 (ng/ml)
0.3279
E
Aggregation (%)
0.4272
0.8904
0.4530
unstimulated
Collagen
Thrombin
F
HSP47 (ratio, MFI)
Time (days)
HSP47 expression (ratio, MFI)
0.0112
0.0012
0.4765
Baseline
d 4-5
d 9-10
CD42b (ratio, MFI)
Time (day)
Cd42b (ratio, MFI)
0.3167
0.9900
0.2602
Glycoprotein VI (ratio, MFI)
Time (day)
0.1017
0.5156
0.5356
G
GPVI (MFI)
0.4356
GPIbα (MFI)
0.2193
Baseline
d 27
H
d1
d27
HSP47
GAPDH
Immobilized 1
Immobilized 2
Immobilized 3
HSP47 level (normalized to GAPDH)
0.0015

Fig. S6. Analysis of patients with SCI and bed rest study participants

(A) Platelet surface expression of glycoprotein (GP) VI and Ibα was determined using flow cytometry (n = 8; bars show means ± SD; p-values were determined using unpaired t-test). (B) Clotting time and mean clot firmness in whole blood from patients with SCI and respective controls were quantified by whole blood thromboelastography after INTEM, EXTEM and FIBTEM activation (n = 8; bars show means ± SD; p-values were determined using Mann-Whitney test for clotting time Extem and Fibtem and mean clot firmness Fibtem; unpaired t-test was used for clotting time Intem and mean clot firmness Extem and Intem). (C) Plasma coagulation parameters (INR and aPTT) were determined (n = 10; bars show means ± SD; p-values were determined using unpaired t-test for aPTT and Mann-Whitney for INR). (D) Circulating DNA and citrullinated histone 3 (CitH3) plasma levels were analyzed (n = 8; bars show means ± SD; p-values were determined using unpaired t-test for CitH3 and circulating DNA). (E) Maximum aggregation response of washed platelets was assessed after stimulation with the indicated stimuli ($n \geq 7$; bars show means ± SD; p-values were determined using Mann-Whitney test for unstimulated and thrombin; unpaired t-test for collagen). (F) Serial analysis of HSP47 and platelet markers of acutely immobile patients at indicated time points is shown (symbols represent single individuals; n = 6 per group; bars show means ± SD; p-values were determined using one-way Anova). (G) Serial analysis of glycoprotein (GP) VI and Ibα expression of bed rest participants at indicated time points is shown (symbols represent single individuals; n = 10 per group; p-values were determined using paired t-test). (H) Representative immunoblots for HSP47 in platelets of three individuals at baseline (day 1) and after 27 days of bed rest. Relative HSP47 levels normalized to GAPDH are shown; bars show means ± SD, p-values were determined using paired t-test.

No.	Bear	Age (y)	Sex	Cause of death	Pulmonary embolism
1	439/18	41	f	pancreatic cancer	no
2	83/17	32	f	unknown - weakness after hibernation	no
3	848/14	21	m	collapse after anaesthesia, atherosclerosis	no
4	505/13	23	f	lymphoma	yes
5	383/12	adult	f	unknown - found dead in hamlet - several organ bleedings	no
6	1154/11	27	m	unknown - ataxia	yes
7	860/08	25	f	death after anaesthesia and transport from Croatia to Germany	no
8	898/06	adult	m	unknown - hyperaemia	no
9	315/04	0.3	m	pleuritis	yes
10	582/02	2	f	adenocarcinoma	no
11	185/94	2	m	lymphosarcoma	no

Table S1. Pulmonary embolism in brown bears undergoing autopsy

Baseline characteristics, cause of death and presence of pulmonary embolism in bears in captivity are shown.

Table S2. Proteome comparison of bear and human lung thrombi from LCM
(provided separately in Excel format)

		Control (n=23)	SCI (n=23)	p-value
Age	ys	50.5±19.3	50.2±18.1	0.9625
Male sex	%	87.0	87.0	
WBC	10^9/l	6.6±1.7	6.5±2.4	0.8244
NEUT*	%	57.2±7.4	64.3±8.1	**0.0202**
HGB	g/dl	14.8±1.5	13.1±2.2	**0.0044**
HCT	%	42.9±4.1	38.4±6.0	**0.0043**
PLT	10^3/l	259±70	246±60	0.4945
MPV	fl	10.3±1.2	10.9±0.9	0.0945
Krea	mg/dl	1.0±0.2	0.8±0.6	**0.0022**
GOT	U/l	28.0±13.8	25.9±18.6	0.2507
CRP	mg/dl	0.4±0.8	1.5±2.1	**0.0028**
Antithrombotic therapy				
Apixaban	%	4.3	4.3	
Aspirin	%	21.7	21.7	
Clopidogrel	%	4.3	4.3	
Level of injury (ISNCSCI)				
C2	%	0	4.3	
C3	%	0	8.7	
C4	%	0	21.7	
C5	%	0	21.7	
C6	%	0	21.7	
T7	%	0	4.3	
T10	%	0	4.3	
T12	%	0	4.3	
L1	%	0	4.3	
L2	%	0	4.3	
Time since injury				
9 - 12 months	%	0	4.3	
1 - 10 years	%	0	34.8	
> 10 years	%	0	60.9	

Table S3. Baseline characteristics of patients with SCI

Baseline characteristics of patients with SCI and healthy controls are shown (n = 23; * n = 14; p-values were determined using unpaired t-test (age, neutrophils (NEUT), platelets (PLT), MPV) or Mann-Whitney test (hemoglobin (HGB), hematocrit (HCT), white blood cells (WBC), CRP, GOT, creatinine (KREA)).

Age	ys	67.8±13.2		
Male sex	%	33.3		
		Baseline	**d 4-5**	**d 9-10**
WBC	10^9/l	16.2±7.8	11.8±0.9	12.8±5.7
HGB	g/dl	12.2±1.9	10.6±2.0	10.0±2.1
HCT	%	36.1±5.4	32.6±6.3	30.4±6.0
PLT	10^3/l	223±38	215±33	289±27
MPV	fl	10.2±0.7	10.5±0.9	10.7±0.7
Krea	mg/dl	0.8±0.2	0.7±0.2	0.6±0.1
GOT	U/l	23.5±10.3	22.2±5.2*	39.4±29.6
CRP	mg/dl	3.4±3.9	3.6±3.1	3.0±1.7
Antithrombotic therapy		%	0	
Cause of immobility				
Subarachnoid haemorrhage		%	50	
Subdural haematoma		%	16.7	
Occlusion of Arteria basilaris		%	16.7	
Intracerebral haemorrhage		%	16.7	

Table S4. Baseline characteristics of acutely immobile patients

Baseline characteristics of acutely immobile patients are shown; n = 6; * n = 5.

Table S5. Human bed rest to bear seasonal comparison protein list
(provided separately in Excel format)

REAGENT	SOURCE	IDENTIFIER
Antibodies		
Human/Mouse Myeloperoxidase/MPO Antibody	R&D systems	Cat# AF3667; RRID: AB_2250866
Anti-Histone H3 antibody	Abcam	Cat# ab18251
Polyclonal Rabbit Anti-Human Fibrinogen	DAKO	Cat# A0080; RRID: AB_2894406
HSP47 Antibody	Novus	Cat# NBP1-97491-0.05mg; RRID: AB_11189622
HSP47 Antibody (G-12) FITC	Santa Cruz Biotechnology	Cat# sc-5293; RRID: AB_627757
Thrombin Antibody (F-1)	Santa Cruz Biotechnology	Cat# sc-271449; RRID:AB_10676669
normal mouse IgG2a-FITC	Santa Cruz Biotechnology	Cat# sc-2856; RRID: AB_737238
Goat Anti-Mouse IgG (H + L)-HRP	Bio-Rad	Cat# 1706516; RRID: AB_2921252
β-Actin (13E5) Rabbit mAb (HRP Conjugate)	Cell Signaling Technology	Cat# 5125; RRID: AB_1903890
GAPDH Monoclonal Antibody (1D4)	Invitrogen	Cat# MA1-16757; RRID: AB_568547
PE/Cyanine5 anti-human CD41 Antibody	Biolegend	Cat# 303708; RRID: AB_314378
FITC anti-human CD16 Antibody	Biolegend	Cat# 302006; RRID: AB_314206
Alexa Fluor® 647 anti-human CD41/CD61 Antibody	Biolegend	Cat# 362806; RRID: AB_2566476
Alexa Fluor® 700 anti-human CD62P (P-Selectin) Antibody	Biolegend	Cat# 304932; RRID: AB_2687351
PE/Dazzle™ 594 anti-human CD61 Antibody	Biolegend	Cat# 336426; RRID: AB_2832659
Brilliant Violet 650™ anti-human CD42b Antibody	Biolegend	Cat# 303926; RRID: AB_2715927
Brilliant Violet 510™ anti-human CD154 Antibody	Biolegend	Cat# 310830; RRID: AB_2563833
APC/Cyanine7 anti-human CD63 Antibody	Biolegend	Cat# 353046; RRID: AB_2860923
Brilliant Violet 605™ anti-human CD11b Antibody	Biolegend	Cat# 301332; RRID: AB_2562021
FITC anti-human CD16 Antibody	Biolegend	Cat# 302006; RRID: AB_314206
PE anti-mouse CD45.1 Antibody	Biolegend	Cat# 110708; RRID: AB_313497
APC/Cyanine7 anti-mouse CD45.2 Antibody	Biolegend	Cat# 109824; RRID: AB_830789
PE Mouse Anti-Human CD29	BD Bioscience	Cat# 555443; RRID: AB_395836

BV421 Mouse Anti-Human Platelet GPVI	BD Bioscience	Cat# 743941; RRID: AB_2741863
Chemicals, peptides, and recombinant proteins		
Col003	MedChemExpress	Cat# HY-124817
HSP47 small molecule inhibitor RH00007SC	Thermo fisher scientific	Cat# RH00007SC
2′,7′-Dichlorodihydrofluorescein diacetate	Sigma-Aldrich	Cat# D6883
Phorbol 12-myristate 13-acetate	Sigma-Aldrich	Cat# P8139
Lipopolysaccharides from Escherichia coli O127:B8	Sigma-Aldrich	Cat# L3129
FORMYL-MET-LEU	Sigma-Aldrich	Cat# F3506
Thrombin	Chrono-Log	Cat# P/N386
Collagen	Chrono-Log	Cat# P/N385
Heat Shock Protein 47 Recombinant Human	USBiological life scineces	Cat# H1834-20E.100
Critical commercial assay		
Pan Monocyte Isolation Kit, human	Miltenyi Biotec	Cat# 130-096-537
MACSxpress® Whole Blood Neutrophil Isolation Kit, human	Miltenyi Biotec	Cat# 130-104-434
Pan T Cell Isolation Kit, human	Miltenyi Biotec	Cat# 130-096-535
Pan B Cell Isolation Kit, human	Miltenyi Biotec	Cat# 130-101-638
Neutrophil Isolation Kit, mouse	Miltenyi Biotec	Cat# 130-097-658
Pan T Cell Isolation Kit II, mouse	Miltenyi Biotec	Cat# 130-095-130
Monocyte Isolation Kit (BM), mouse	Miltenyi Biotec	Cat# 130-100-629
Pan B Cell Isolation Kit II, mouse	Miltenyi Biotec	Cat# 130-095-813
circulating DNA quantification kit,	Abcam	Cat# ab156898
Citrullinated Histone H3 (Clone 11D3	Cayman	Cat# 501620
Cell Death Detection ELISA PLUS Kit	Roche	Cat# 50-100-3308
Prostacyclin ELISA Kit	AVIVA Systems Biology	Cat# OKEH02555

Table S6. List of reagents